


Article

Heavy-Ion Fusion Reaction Calculations: Establishing the Theoretical Frameworks for ^{111}In Radionuclide over the Coupled Channel Model

Zehra Merve Cinan ^{1,*}, Burcu Erol ², Taylan Baskan ¹ and Ahmet Hakan Yilmaz ¹

¹ Department of Physics, Faculty of Sciences, Karadeniz Technical University, Trabzon 61080, Turkey; taylanbaskan@ktu.edu.tr (T.B.); hakany@ktu.edu.tr (A.H.Y.)

² Department of Physics, Faculty of Arts and Sciences, Recep Tayyip Erdoğan University, Rize 53100, Turkey; burcu.karayunus@erdogan.edu.tr

* Correspondence: m_cinan@ktu.edu.tr; Tel.: +90-462-377-4136

Abstract: In this work, the production of ^{111}In radionuclide has been investigated theoretically via heavy-ion fusion reactions of two stable nuclei: $^{37}\text{Cl} + ^{74}\text{Ge}$, $^{26}\text{Mg} + ^{85}\text{Rb}$, $^{30}\text{Si} + ^{81}\text{Br}$, and $^{46}\text{Ca} + ^{65}\text{Cu}$ reactions. Fusion cross-sections, barrier distributions, and potential energies on mutual orientations in the reactions planes of all reactions have been researched in detail around the barrier region via a coupled channel (CC) model using different codes. First of all, the most suitable codes and calculation parameter sets were determined through the $^{37}\text{Cl} + ^{74}\text{Ge}$ reaction, whose experimental data were available. The compatibility of the calculations via NRV knowledge base, CCFULL, CCDEF codes, and Wong's formula with experimental data was analyzed. Barrier distributions and cross-sections for heavy-ion fusion reactions have been investigated with miscellaneous codes and vibrational-rotational nuclei combinations for interacting nuclei. Afterward, calculations were made with the determined parameter values for new reaction suggestions ($^{26}\text{Mg} + ^{85}\text{Rb}$, $^{30}\text{Si} + ^{81}\text{Br}$, and $^{46}\text{Ca} + ^{65}\text{Cu}$ reactions) and the results were compared. This study aims to suggest the new reaction combinations for the production of ^{111}In radionuclide, to explore the impacts of different calculation codes and nuclear parameter combinations on the heavy-ion fusion cross-sections and barrier distributions, to demonstrate that the results are reliable, and to emphasize the importance of developing these studies in the preparation of new experiments.

Keywords: barrier distributions; coupled channel (CC) model; cross-sections; heavy-ion fusion; indium-111; mutual orientation; potential energy; radionuclide



Citation: Cinan, Z.M.; Erol, B.; Baskan, T.; Yilmaz, A.H. Heavy-Ion Fusion Reaction Calculations: Establishing the Theoretical Frameworks for ^{111}In Radionuclide over the Coupled Channel Model. *Energies* **2021**, *14*, 8594. <https://doi.org/10.3390/en14248594>

Academic Editor: Ruben Otin

Received: 14 November 2021

Accepted: 15 December 2021

Published: 20 December 2021

Publisher's Note: MDPI stays neutral with regard to jurisdictional claims in published maps and institutional affiliations.



Copyright: © 2021 by the authors. Licensee MDPI, Basel, Switzerland. This article is an open access article distributed under the terms and conditions of the Creative Commons Attribution (CC BY) license (<https://creativecommons.org/licenses/by/4.0/>).

1. Introduction

The interaction between heavy ions is simply defined as the interaction of two nuclei moving at a central potential of a short-orbit nuclear interaction and a long-orbit Coulomb repulsive effect [1–3]. The fusion reactions of heavy ions have attracted the attention of nuclear physicists, who have subsequently performed theoretical and experimental studies in recent years [4–7]. This enhancement in attention is owing to the day-by-day increase in heavy-ion accelerator research areas with wide and usable energy intervals. These heavy-ion reactions also offer the possibility to produce excited nuclei. With the emergence of heavy-ion reactions, nuclear physics has taken on a new dimension [8–10]. To understand the inner structure and nuclear properties of the nucleus, many types of research have been, and continue to be, carried out in this field [11–15]. All this research leads to the development of nuclear models that aim to explain the structure of the nucleus. However, the interaction of nuclei and reaction components are very complex and difficult to understand concepts. Obtaining heavy-ion nuclei from particle accelerators has provided many possibilities for understanding the complexities of the nuclear structure together with heavy-ion reaction dynamics. Experimental research to obtain fusion cross-sections

has provided evidence of the importance of coupled channel effects at the energy district near the Coulomb barrier. Improvements on this model (CC) have facilitated an ideal explanation of the fusion excitation function characteristic in the barrier region [16–18]. Heavy-ion fusion reactions on a large interval (above and under) of the barrier, where coupling effects are strongest and coupling channels are workable, are investigated by the coupled channel method. At regions significantly over the barrier, too many channels have to be taken into account, which eliminates the possibility of examining the channels individually. This model is a convenient and time-saving method to easily perform calculations for all channels. A coupled channel (CC) model was created by including degrees of freedom in the overall calculation framework of heavy-ion fusion. This model has not only triumphantly explained the fusion cross-sections for many reaction systems in a more practical approach, but has also provided researchers with an existing interpretation called heavy-ion fusion barrier distributions.

The dynamics required for fusion reactions are managed via quantum tunneling, thanks to a Coulomb barrier. In heavy-ion fusion reactions, compound nuclei come into existence thereafter crossing a fusion barrier formed among the repulsive Coulomb and the nuclei from attractive nuclear forces. This process occurs when the motion is particularly dependent on degrees of freedom, vibrations of nuclear surfaces, rotation of deformed nuclei, and nucleon transfer. The fusion cross-section is also bound up with the ground state shape of the nuclei. If the projectile and target nuclei are spherical, exceeding the fusion barrier is easier; however, if deformed cores are used, the barrier problem becomes a little more complicated. The effect on the heavy-ion fusion calculations of deformations or rotation of deformed nucleus in the coupled channel (CC) approach has been investigated and expressed in a lot of work over the years [19–23]. Many theoretical approaches, which are widely used today and which especially take into account the dynamics of nucleus–nucleus interactions, have been improved through research. Some of these contain the optical model in elastic scattering and the CC formula to compute fusion cross-sections. Many code packs are written in the Fortran language and have a complex user interface; the researchers must accurately prepare input files, which will consist of many lines. In other words, a non-expert user would encounter serious difficulties while using these codes and subsequently waste time.

Many exclusive nuclei are widely used for diagnostic or therapeutic intentions in medical applications. The ^{111}In radionuclide is one of these exclusive nuclei. This important nucleus is generally bred from the reactions induced via protons on Ag (silver) or Cd (cadmium) and it has a ≈ 2.81 days half-life. It is substantial for the future of research in both nuclear physics (in nuclear energy and nuclear engineering) and nuclear medicine implementations to make suggestions that will shed light on alternative production means of significant nuclei such as ^{111}In . In addition to the existing production methods, some suggestions can be developed for its investigation with the help of heavy-ion fusion reactions. Substantial research on the example of the production mechanism of In-111 radionuclide by sub-barrier fusion reaction was carried out by E. Martinez-Quiroz et al. (2001). They examined the eventual influences of phonon states for vibrational (spherical) nuclei, their deformation, and nucleon transfer for rotational (deformed) nuclei, and thus analyzed the barrier distributions showing their consistency with the available degrees of freedom.

In this research, we focused on establishing the theoretical frameworks for ^{111}In radionuclide over the coupled channel model in the heavy-ion fusion reaction calculations. Our aim in the study is to show the reader the compatibility or incompatibility between codes and numerical calculation methods when compared with experimental data. If there is no experimental data for the studied reaction group then, in order to have important details as regards the fusion cross-sections with the calculations made and with the use of different methods, one must determine how the similarities and differences between the methods affect the results. For this aim, we explored the impacts of different calculation codes and nuclear parameter combinations on the fusion cross-sections, barrier distributions, and potential energies on mutual orientations in the reactions planes for the ^{111}In

radionuclide. Therefore, our research was focused on seeing in more detail the effect of different coupled channel codes (NRV, CCFULL, CCDEF codes, and Wong's formula), as well as nuclear parameter combinations (such as deformation or vibration characteristics) of the projectile and target nuclei on the cross-section [22–29]. In the second part, information about the coupled channel (CC) model used is given. All of the code analyses of experimental data and calculation results are represented in the third part. In the last part, general synopsis and the consequences of our work are submitted [30–36].

2. Coupled Channel (CC) Model

In this part, we have abridged and explained the CC model that we used in our computations for all of our reactions, taking into account important details.

In the coupled-channel model, coupled channel equations are established for relative motion of the nuclei, including all relating channels, such as rotational and vibrational excitations; the CC equalities are analyzed via the incoming wave boundary condition around the Coulomb barrier. Assuming that the nuclear potential has a Woods–Saxon form, the depth is determined to form fusion cross-sections.

Barrier distribution function, $D(B)$, is expressed as follows at the classical limits [28]:

$$D(B) = \frac{1}{\pi R_B^2} d^2(E\sigma_{\text{fus}})/dE^2|_{E=B} \quad (1)$$

Here B is the barrier height, R_B is the barrier radius or barrier position, σ_{fus} is fusion cross-sections, and E is the incident energy, these parameters also can be viewed in the elaboration in Table S1 (this table can be viewed in the Supplementary Information File; Table S1).

$D(B)$ is associated with the advanced penetration characteristics of the barrier in important channel couplings. If the barrier penetration probability symbolized as $T_1(B; E)$ is explained with the Hill–Wheeler formula [29]:

$$x = B + \frac{\hbar^2}{2\mu R_B^2} l(l+1) - E \quad (2)$$

$$T_1(B; E) = f(x) \quad (3)$$

Here x is the function argument that defines the relevant parameters, B is the barrier height, \hbar is the modified form of Planck's constant called h-bar (namely; $\hbar = h/2\pi$), μ is the reduced mass of the system, l is the angular momentum, R_B is the barrier radius or barrier position, these parameters also can be viewed in the elaboration in Table S1 (this table is explained in the Supplementary Information File; Table S1).

Reaction cross-sections can be written:

$$\sigma_{\text{fus}}(E) = \frac{\pi \hbar^2}{2\mu E} \sum_{l=0}^{\infty} (2l+1) T_1(E) \quad (4)$$

If the function $D(B)$ is rearranged according to Equation (4) [20]:

$$\frac{d(E\sigma_{\text{fus}})}{dE} = \frac{\pi \hbar^2}{2\mu} \sum_{l=0}^{\infty} (2l+1) \frac{dT_1(B; E)}{dE} = -\pi R_B^2 \sum_{l=0}^{\infty} (2l+1) \frac{dT_1(B; E)}{dl} \quad (5)$$

According to Rowley et al., the barrier distribution function may be expressed via the second derivative of the fusion cross-section function in the following form:

$$D(E) = \delta(E - B) = \frac{1}{\pi R_B^2} \frac{d^2(E\sigma_{\text{fus}})}{dE^2} = \frac{dT_{l=0}(B; E)}{dl} \quad (6)$$

where last equality results from Equation (4), $T(E) = 1$ for $E > B$ and $T(E) = 0$ for $E < B$. All factors included in these equations are listed and described lengthily in Table S1.

Because the potential energies are large-scale, the coming flux passes the barrier value at varying heights B (various deformation parameters). The barrier distribution is associated with the relative motion, which creates a potent coupling between the rotational and the vibrational states in combining the internal degrees of freedom in projectile–target nuclei combinations. While the rotational state of the nuclei is related to their deformations, the vibrational states are linked with variations in the forms of the nuclei. When the projectile and target nuclei meet and interact in a certain region, the surface of these reacting nuclei may be disrupted owing to the various and different effects of nuclear forces. This process is called the deformation of the nuclei [1].

The fusion cross-sections are calculated with Equation (4) in the limits of coupled channel (CC) model [1]. Computation of the compound nucleus (CN) cross-sections in the interactions of the heavyweight nuclei, is expressed as follows:

$$\sigma_{\text{fus}}^{\text{CN}}(E) = \frac{\pi\hbar^2}{2\mu E} \sum_{l=0}^{\infty} (2l+1) T_l(E) P_{\text{CN}}(E, l) \quad (7)$$

here $P_{\text{CN}}(E, l)$ is expressed as the penetration prospect of the CN, these parameters also can be viewed in the elaboration in Table S1 (this table can be viewed in the Supplementary Information File; Table S1).

Wong's formula for cross-sections is expressed as follows [26]:

$$\sigma(E) = \frac{\hbar\omega}{2E} R_B^2 \ln \left[1 + \exp \left(\frac{2\pi}{\hbar\omega} (E - V_B) \right) \right] \quad (8)$$

here $\hbar\omega$ is the curvature is, R_B is the barrier radius, and V_B is the barrier potential, these parameters also can be viewed in the elaboration in Table S1 (this table can be viewed in the Supplementary Information File; Table S1). In Equation (8) we can write these expressions for special cases:

$$\sigma(E) = \pi R_B^2 \left(1 - \frac{V_B}{E} \right) \text{ for } E > V_B \quad (9)$$

$$\sigma(E) \approx R_B^2 \frac{\hbar\omega}{2E} \exp \left(\frac{\hbar\omega}{2E} (E - V_B) \right) \text{ for } E < V_B \quad (10)$$

The subsequent statement relates to Wong's barrier distributions formula:

$$\frac{d^2 E \sigma_{\text{fus}}}{dE^2} = \pi R_B^2 \frac{2\pi}{\hbar\omega} \frac{e^x}{(1 + e^x)^2}; x = \frac{2\pi}{\hbar\omega} (E - V_B) \quad (11)$$

The model applied in all codes is nearly the same. Mathematical (numerical) realizations are different in some details and the other differences between the NRV, CCFULL, and CCDEF; the NRV applies a more accurate scheme for the matrix element calculation; it also provides the possibility to work with the proximity potential, take into account the so-called geometrical factor in the potential that is quite important when large deformations play a role and it provides a convenient interface. Namely, although the NRV, CCFULL, and CCDEF seem the same in terms of input and output, the biggest feature that distinguishes them from each other is the matrix element calculation forms [22–27]. NRV is a new algebraic method, used for the numerical solution of the Schrödinger equation group combined in fusion reactions. To acquire an accurate barrier distribution, right and high-quality fusion cross-section data is needed, as well as a beneficial numerical method to compute the second derivative. With this motivation, we compared the fusion barrier distributions obtained via various codes. To obtain an accurate fusion barrier distribution, accurate and high-quality fusion cross-sections value is required, as well as a good numerical method to calculate the second derivative. For this purpose, we compared the fusion barrier distributions obtained by theoretical calculations using the NRV code. The second derivative of Wong's formula is a model that reproduces the experimental data. The

work shows that Wong's formula again produced the barrier distribution in an admissible attitude checked against theoretical calculations.

3. Results of The Heavy-Ion Fusion Cross-Sections, Barrier Distributions, and Potential Energies on Mutual Orientations in the Reactions Planes

All of our calculations which were also introduced in graphical and table form were made with the NRV knowledge base, CCFULL, CCDEF codes, and Wong's Formula [22–27]. The choice of potential parameters is very important for the reliability of the results. Firstly, we set our parameters according to experimental data and then rearranged each parameter for coupled channel model and dynamic deformations and rotation set. The indicated experimental data were taken from reference [30]. For the CC model, we took all coupled channel parameters from references [31–35]. Then we itemized Woods–Saxon potential parameters used in the nucleus–nucleus interactions. In this work, it should be exclusively underlined that ^{74}Ge , ^{26}Mg , ^{85}Rb , ^{30}Si , ^{81}Br , and ^{65}Cu nuclei are deformed ones that have to be treated as rotators; besides this ^{37}Cl and ^{46}Ca nuclei are treated as having the vibrational intrinsic spectra in Table 1.

Table 1. Heavy-ion fusion reactions coupling parameter details in the CC model calculations.

Vibrational Nucleus States					
Nucleus	J^π	E^* (MeV)	β_{2+}	β_{3-}	References
^{37}Cl	$1/2^+$	1.7266	0.1400		[30–35]
	$5/2^+$	3.0861	0.2400		[30–35]
	$7/2^-$	3.1035		0.3200	[30–35]
	$9/2^-$	4.0100		0.3300	[30–35]
^{46}Ca	0^+	1.3460	0.1468		[30–35]
	0^+	3.6140		0.2040	[30–35]
Rotational (Deformed) Nucleus States					
Nucleus	J^π	E^* (MeV)	β_2	β_4	References
^{74}Ge	0^+	0.5959	−0.2370	−0.0360	[30–35]
^{26}Mg	0^+	1.8087	−0.3510	0.1620	[30–35]
^{85}Rb	$5/2^-$	0.1512	0.0640	−0.0100	[30–35]
^{30}Si	0^+	2.2353	−0.2360	0.0400	[30–35]
^{81}Br	$3/2^-$	0.2760	0.1400	−0.0300	[30–35]
^{65}Cu	$3/2^-$	1.4818	−0.1250	−0.0050	[30–35]

We have analyzed respectively the $^{37}\text{Cl} + ^{74}\text{Ge}$, $^{26}\text{Mg} + ^{85}\text{Rb}$, $^{30}\text{Si} + ^{81}\text{Br}$, and $^{46}\text{Ca} + ^{65}\text{Cu}$ heavy-ion reaction series cross-sections, barrier distributions, and potential energies on mutual orientations in the reactions planes. The related calculations for all reaction combinations are also given in Figures 1–8. Furthermore, we took the integration parameters as $R_{\text{max}} = 25$ fm and integration step $h = 0.05$ fm in our computations.

3.1. $^{37}\text{Cl} + ^{74}\text{Ge}$ Reaction System Outputs

Firstly we analyzed the calculations of the $^{37}\text{Cl} + ^{74}\text{Ge}$ reaction system with NRV, CCFULL, CCDEF codes, and Wong's formula in the energy range of 60–80 MeV with 0.5 MeV steps [22–27] in Table S2 (this table can be viewed in the Supplementary Information File; Table S2). In Figure 1, the quadrupole vibrational states for the ^{37}Cl nucleus has the following parameters [30–35]: $E^* = 1.7266$ MeV; $\beta_{2+} = 0.1400$. The quadrupole and hexadecapole rotational (deformed) states of the ^{74}Ge nucleus has these deformation parameters, respectively [30–35]: $E^* = 0.5959$ MeV; $\beta_2 = -0.2370$; $\beta_4 = -0.0360$. We regulated the potential parameters as follows: $V_0 = 70$ MeV, $r_0 = 1.220$ fm, and $a_0 = 0.670$ fm for all calculations (in Figure 1a–c) [36].

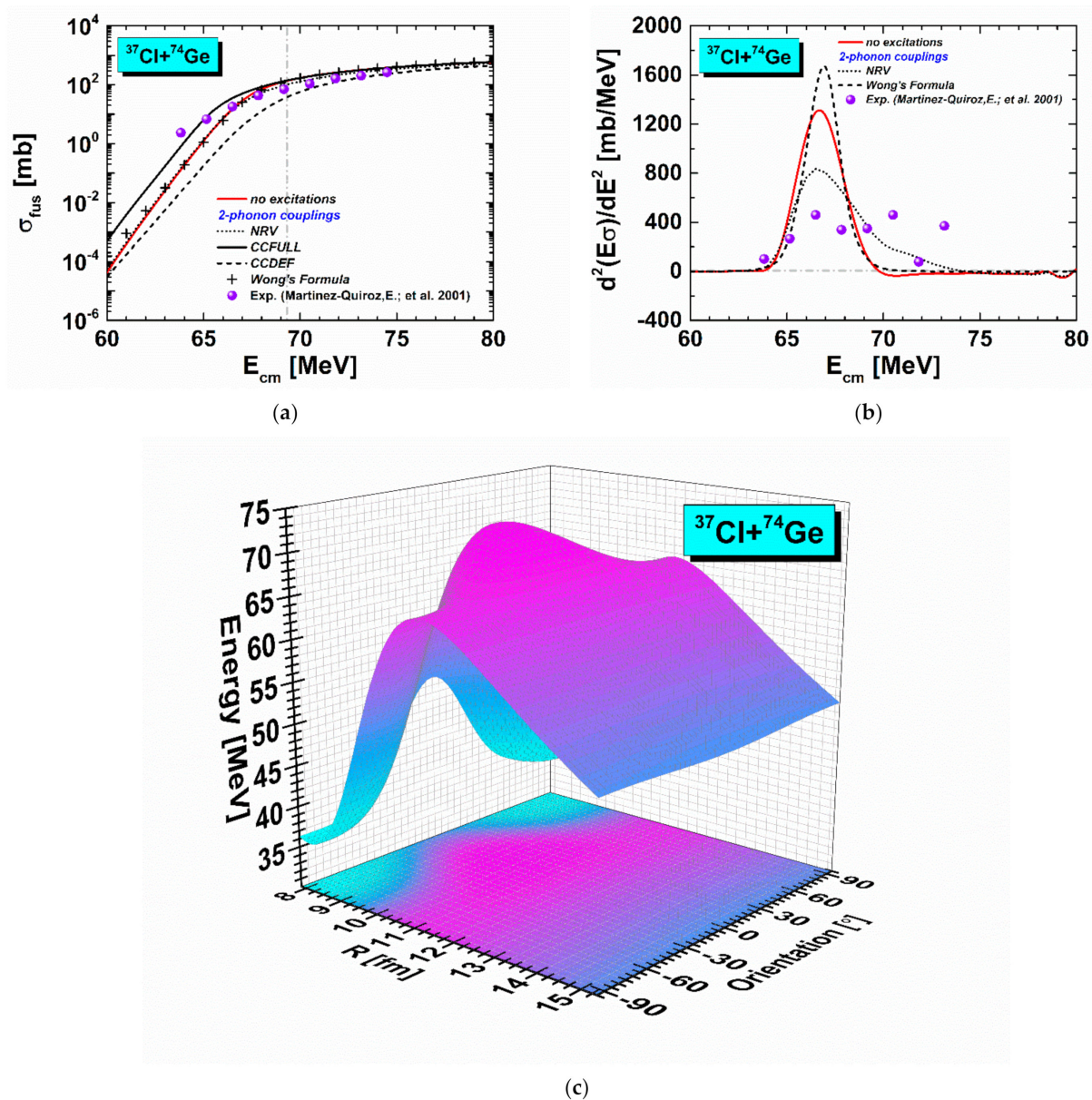


Figure 1. Heavy-ion fusion calculations for $^{37}\text{Cl} + ^{74}\text{Ge}$ (in the quadrupole vibrational state for the ^{37}Cl : $E^* = 1.7266$ MeV; $\beta_{2+} = 0.1400$ and the quadrupole and hexadecapole rotational (deformed) state of the ^{74}Ge : $E^* = 0.5959$ MeV; $\beta_2 = -0.2370$; $\beta_4 = -0.0360$ framework) reaction: (a) cross-sections, (b) barrier distributions, and (c) potential energies on mutual orientations in the reactions plane.

In Figure 1a, for the $^{37}\text{Cl} + ^{74}\text{Ge}$ reaction, cross-section values change from 4.355×10^{-5} mb to 596.8 mb for no excitations calculations. In 2-phonon couplings calculations, values change from 5.086×10^{-5} mb to 542.8 mb for NRV and from 4.975×10^{-4} mb to 601.1 mb for CCFULL, from 3.026×10^{-5} mb to 453.9 mb for CCDEF, and from 1.519×10^{-4} mb to 618.4 mb for Wong's Formula, all values also can be read in the elaboration in Table S2 (this table can be viewed in the Supplementary Information File; Table S2). It should be noted that our calculation outputs bred by all computational models are near one another and in consensus with the experimental outputs. The most substantial distinction was monitored in the CCDEF code in the region below the barrier where we looked at the calculations, the current difference is seen at a negligible level. In the above barrier area, this distinction among the codes was closed and harmony was achieved. Since the deformation parameters cannot be included in Wong's formula calculations, its behavior here shows similar characteristics to the no excitations.

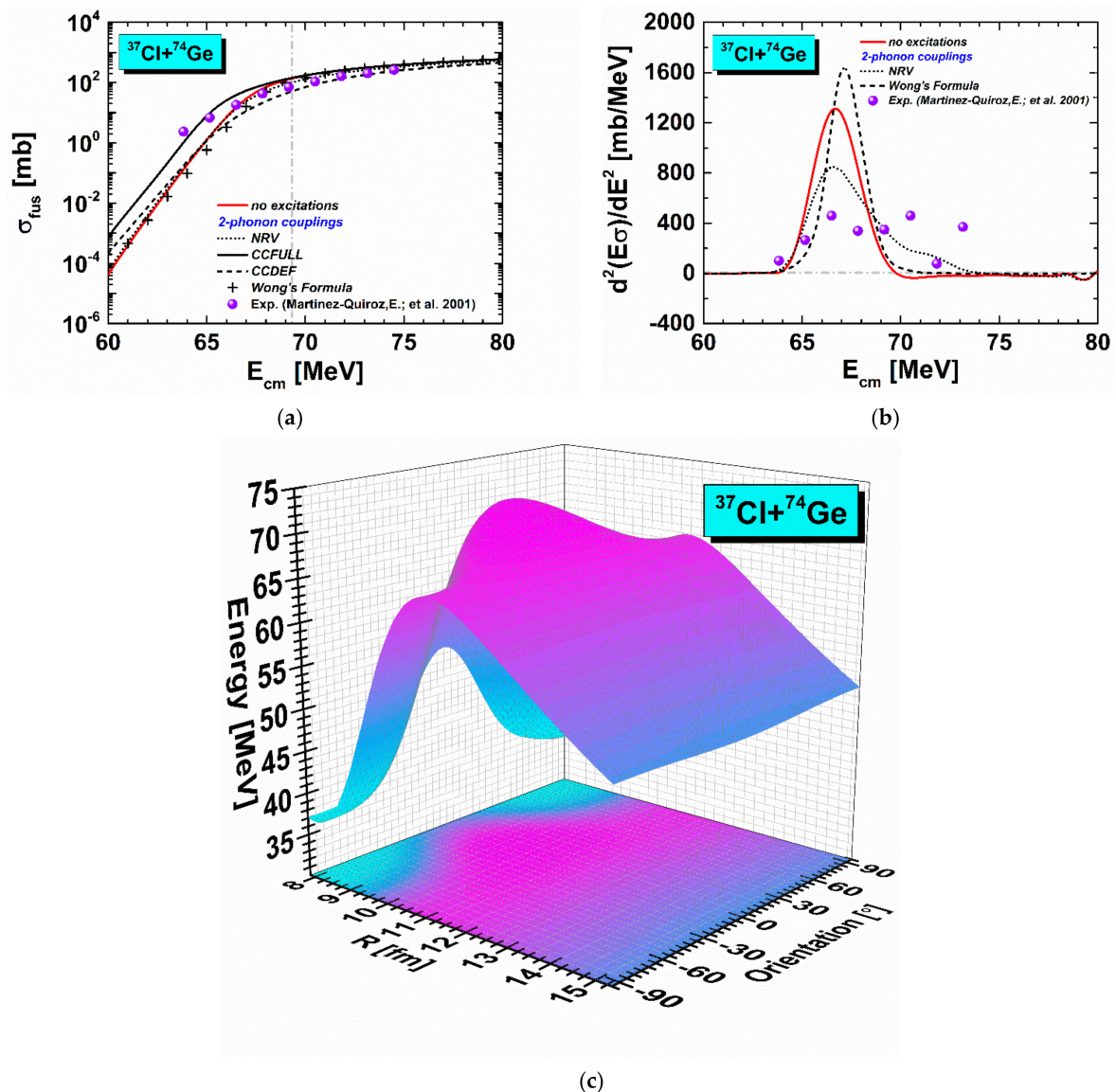


Figure 2. Heavy-ion fusion calculations for $^{37}\text{Cl} + ^{74}\text{Ge}$ (in the quadrupole vibrational state for the ^{37}Cl : $E^* = 3.0861$ MeV; $\beta_{2+} = 0.2400$ and the quadrupole and hexadecapole rotational (deformed) state of the ^{74}Ge : $E^* = 0.5959$ MeV; $\beta_2 = -0.2370$; $\beta_4 = -0.0360$ framework) reaction: (a) cross-sections, (b) barrier distributions, and (c) potential energies on mutual orientations in the reactions plane.

In Figure 1b, for the $^{37}\text{Cl} + ^{74}\text{Ge}$ reaction, barrier distribution values change from 0.010 mb/MeV to 19.130 mb/MeV for no excitations calculations and the highest value was observed as 1298 mb/MeV around the barrier. In 2-phonon couplings calculations, barrier distribution values change from 2.981 mb/MeV to 19.340 mb/MeV for NRV and the highest value was observed as 836.5 mb/MeV around the barrier. The barrier distribution values change from 0.029 mb/MeV to 3.650 mb/MeV for Wong's formula calculations and the maximum value was observed as 1667 mb/MeV around the barrier; all values can also be read in the elaboration in Table S3 (this table can be viewed in the Supplementary Information File; Table S3). In the graph of the barrier distribution function, the data obtained from the NRV and Wong formulas were compared and sharp peaks were observed in almost the same region. The data that showed a good consensus with the experimental outputs were from the NRV. This shows us that both calculations provide reliable results.

Secondly, we analyzed the calculations of the $^{37}\text{Cl} + ^{74}\text{Ge}$ reaction system with NRV, CCFULL, CCDEF codes, and Wong's formula in the energy range of 60–80 MeV with 0.5 MeV steps [22–27]. In Figure 2, the quadrupole vibrational states for the ^{37}Cl nucleus

has the following parameters [30–35]: $E^* = 3.0861$ MeV; $\beta_{2+} = 0.2400$. The quadrupole and hexadecapole rotational (deformed) states of the ^{74}Ge nucleus has these deformation parameters respectively [30–35]: $E^* = 0.5959$ MeV; $\beta_2 = -0.2370$; $\beta_4 = -0.0360$. We regulated the potential parameters as follows: $V_0 = 70$ MeV, $r_0 = 1.210$ fm, and $a_0 = 0.678$ fm for all calculations (in Figure 2a–c) [36].

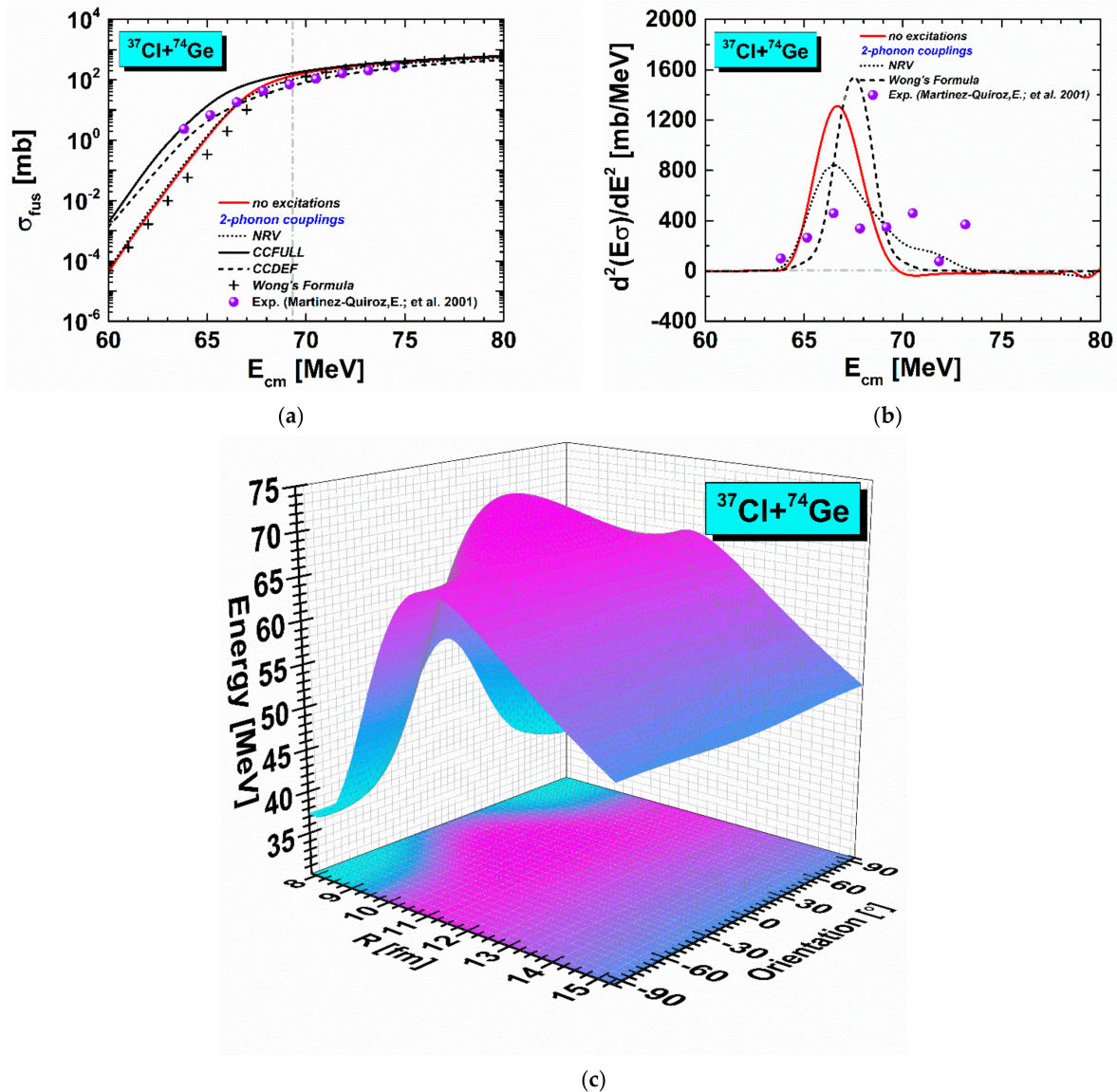


Figure 3. Heavy-ion fusion calculations for $^{37}\text{Cl} + ^{74}\text{Ge}$ (in the octupole vibrational state for the ^{37}Cl : $E^* = 3.1035$ MeV; $\beta_{3-} = 0.3200$ and the quadrupole and hexadecapole rotational (deformed) state of the ^{74}Ge : $E^* = 0.5959$ MeV; $\beta_2 = -0.2370$; $\beta_4 = -0.0360$ framework) reaction: (a) cross-sections, (b) barrier distributions, and (c) potential energies on mutual orientations in the reactions plane.

In Figure 2a, the for $^{37}\text{Cl} + ^{74}\text{Ge}$ reaction, cross-section values change from 4.355×10^{-5} mb to 596.8 mb for no excitations calculations. In 2-phonon couplings calculations, values change from 5.646×10^{-5} mb to 538.6 mb for NRV and from 7.716×10^{-4} mb to 600.9 mb for CCFULL, from 2.187×10^{-4} mb to 458.8 mb for CCDEF, and from 7.673×10^{-5} mb to 594.3 mb for Wong's formula; all values can also be read in the elaboration in Table S4 (this table can be viewed in the Supplementary Information File; Table S4). Our calculation models' outputs are in harmony with each other and with the experimental data. When the deformation parameter value and state of the projectile nuclei were changed, the difference was seen in the previous calculations decreased and perfect harmony was

achieved in the same region in our CCDEF results with other codes. Since the deformation parameters cannot be included in Wong's formula calculations, its behavior here shows similar characteristics to the no excitations.

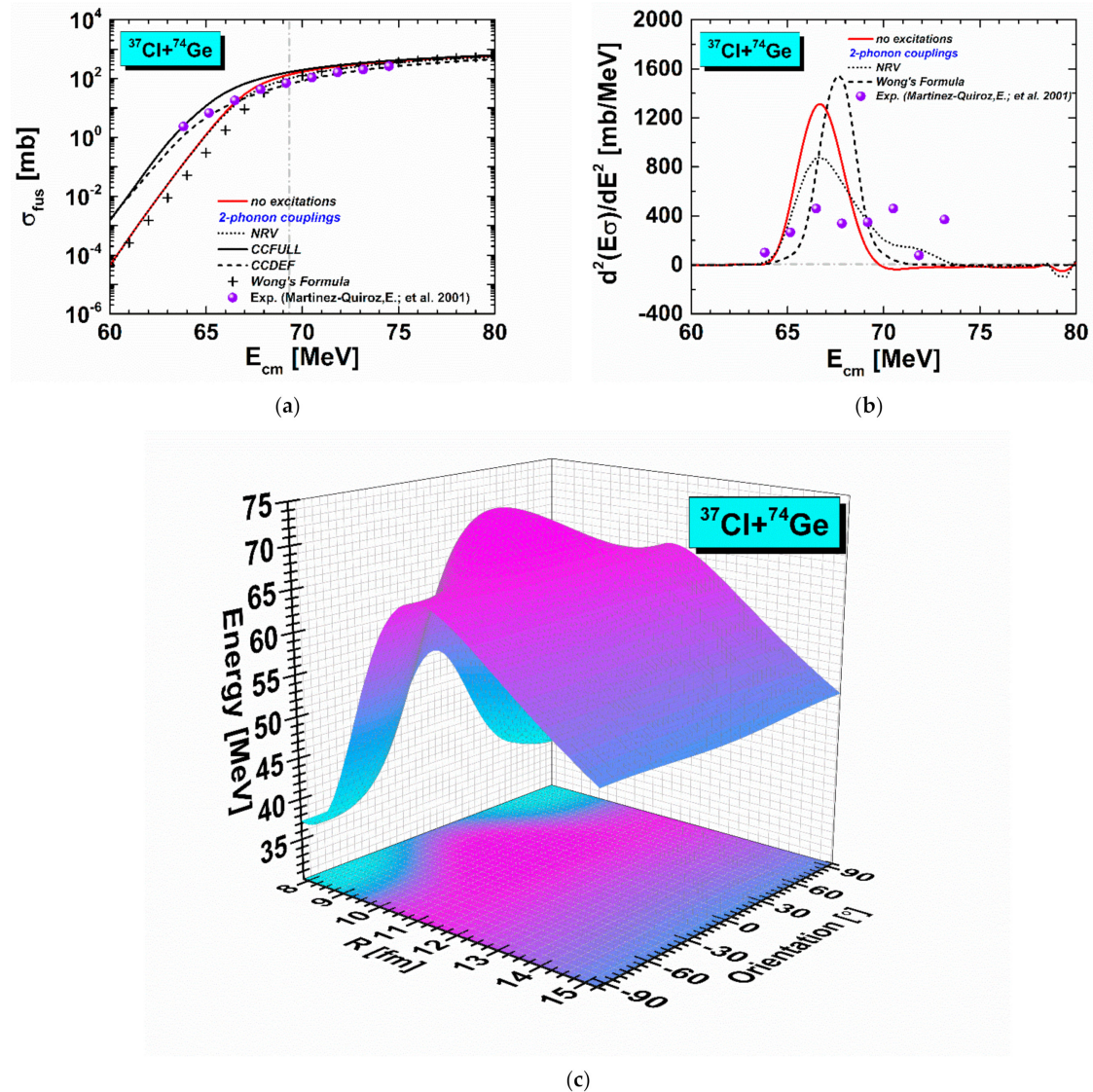


Figure 4. Heavy-ion fusion calculations for $^{37}\text{Cl} + ^{74}\text{Ge}$ (in the octupole vibrational state for the ^{37}Cl : $E^* = 4.0100$ MeV; $\beta_{3-} = 0.3300$ and the quadrupole and hexadecapole rotational (deformed) state of the ^{74}Ge : $E^* = 0.5959$ MeV; $\beta_2 = -0.2370$; $\beta_4 = -0.0360$ framework) reaction: (a) cross-sections, (b) barrier distributions, and (c) potential energies on mutual orientations in the reactions plane.

In Figure 2b, for the $^{37}\text{Cl} + ^{74}\text{Ge}$ reaction, barrier distribution values change from 0.010 mb/MeV to 19.130 mb/MeV for no excitations calculations and the highest value was observed as 1298 mb/MeV around the barrier. In 2-phonon couplings calculations, barrier distribution values change from 0.011 mb/MeV to 22.970 mb/MeV for NRV and the highest value was observed as 856.3 mb/MeV around the barrier. The barrier distribution values change from 0.015 mb/MeV to 6.349 mb/MeV for Wong's formula calculations and the maximum value was observed as 1618 mb/MeV around the barrier, all values also can be read in the elaboration in Table S5 (this table can be viewed in the Supplementary Information File; Table S5). As we observed in our previous calculation, sharp peaks were again viewed in almost the same region. In this calculation, the data showing the best agreement with the experimental data were taken from Wong's formula outputs.

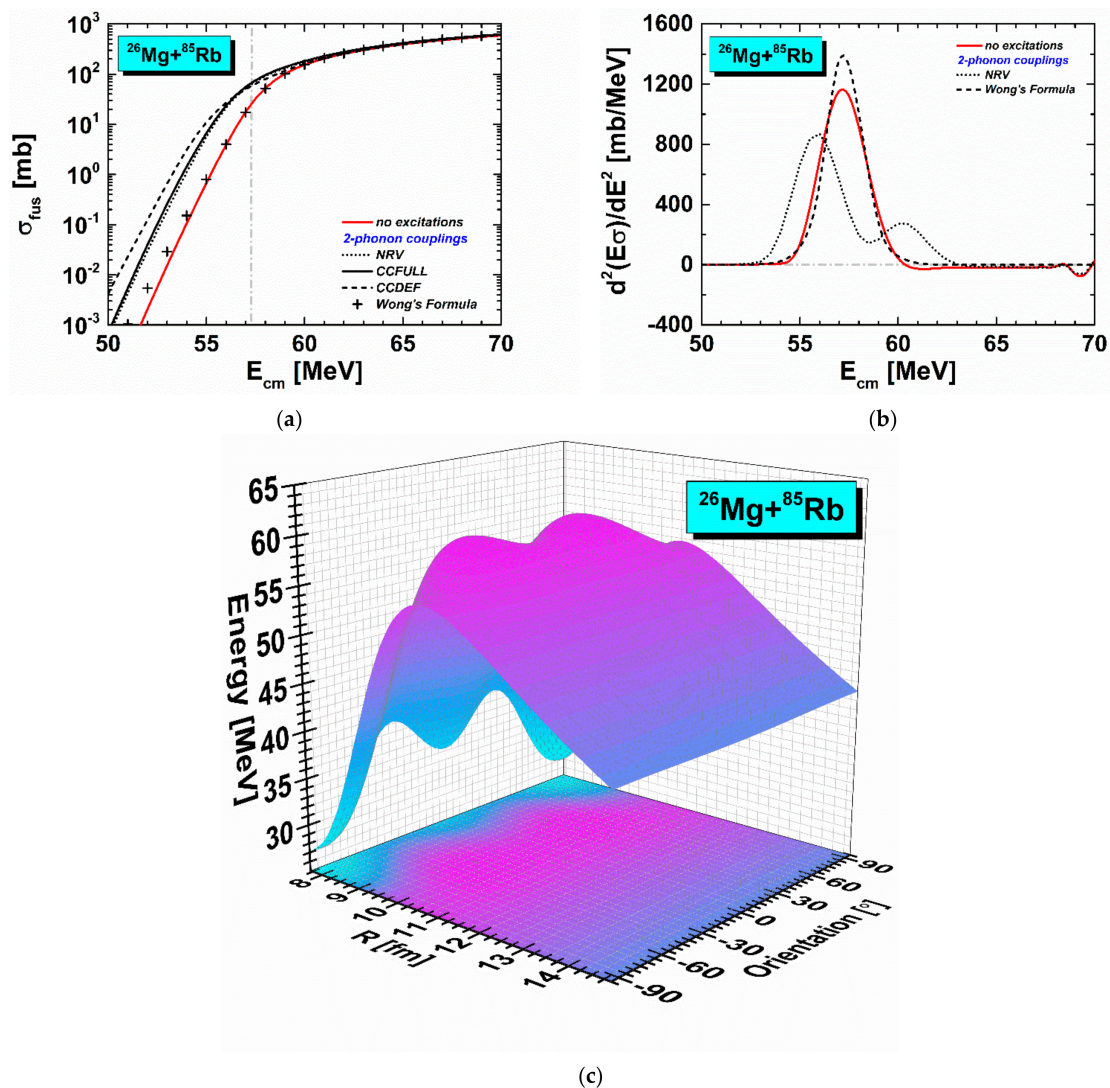


Figure 5. Heavy-ion fusion calculations for $^{26}\text{Mg} + ^{85}\text{Rb}$ (in the quadrupole and hexadecapole rotational (deformed) state for the ^{26}Mg : $E^* = 1.8087$ MeV; $\beta_2 = -0.3510$; $\beta_4 = 0.1620$ and the quadrupole and hexadecapole rotational (deformed) state of the ^{85}Rb : $E^* = 0.1512$ MeV; $\beta_2 = 0.0640$; $\beta_4 = -0.0100$ framework) reaction: (a) cross-sections, (b) barrier distributions, and (c) potential energies on mutual orientations in the reactions plane.

Thirdly we analyzed the calculations of the $^{37}\text{Cl} + ^{74}\text{Ge}$ reaction system with NRV, CCFULL, CCDEF codes, and Wong's formula in the energy range of 60–80 MeV with 0.5 MeV steps [22–27]. In Figure 3, the octupole vibrational states for the ^{37}Cl nucleus has the following parameters [30–35]: $E^* = 3.1035$ MeV; $\beta_{3-} = 0.3200$. The quadrupole and hexadecapole rotational (deformed) states of the ^{74}Ge nucleus has these deformation parameters, respectively [30–35]: $E^* = 0.5959$ MeV; $\beta_2 = -0.2370$; $\beta_4 = -0.0360$. We regulated the potential parameters as follows: $V_0 = 70$ MeV, $r_0 = 1.205$ fm, and $a_0 = 0.675$ fm for all calculations (in Figure 3a–c) [36].

In Figure 3a, for the $^{37}\text{Cl} + ^{74}\text{Ge}$ reaction, cross-section values change from 4.355×10^{-5} mb to 596.8 mb for no excitations calculations. In 2-phonon couplings calculations, values change from 5.025×10^{-5} mb to 541.2 mb for NRV and from 0.002 mb to 614.2 mb for CCFULL, from 0.001 mb to 461.0 mb for CCDEF, and from 4.723×10^{-5} mb to 574.5 mb for Wong's formula; all values also can be read in the elaboration in Table S6 (this table can be viewed in the Supplementary Information File; Table S6). When we evaluated the projectile nuclei in the octupole vibrational state, our CCDEF code calculations approached the CCFULL code. Moreover, in these calculations outputs, the most obvious compatibility with the experimental data was observed in the CCDEF code.

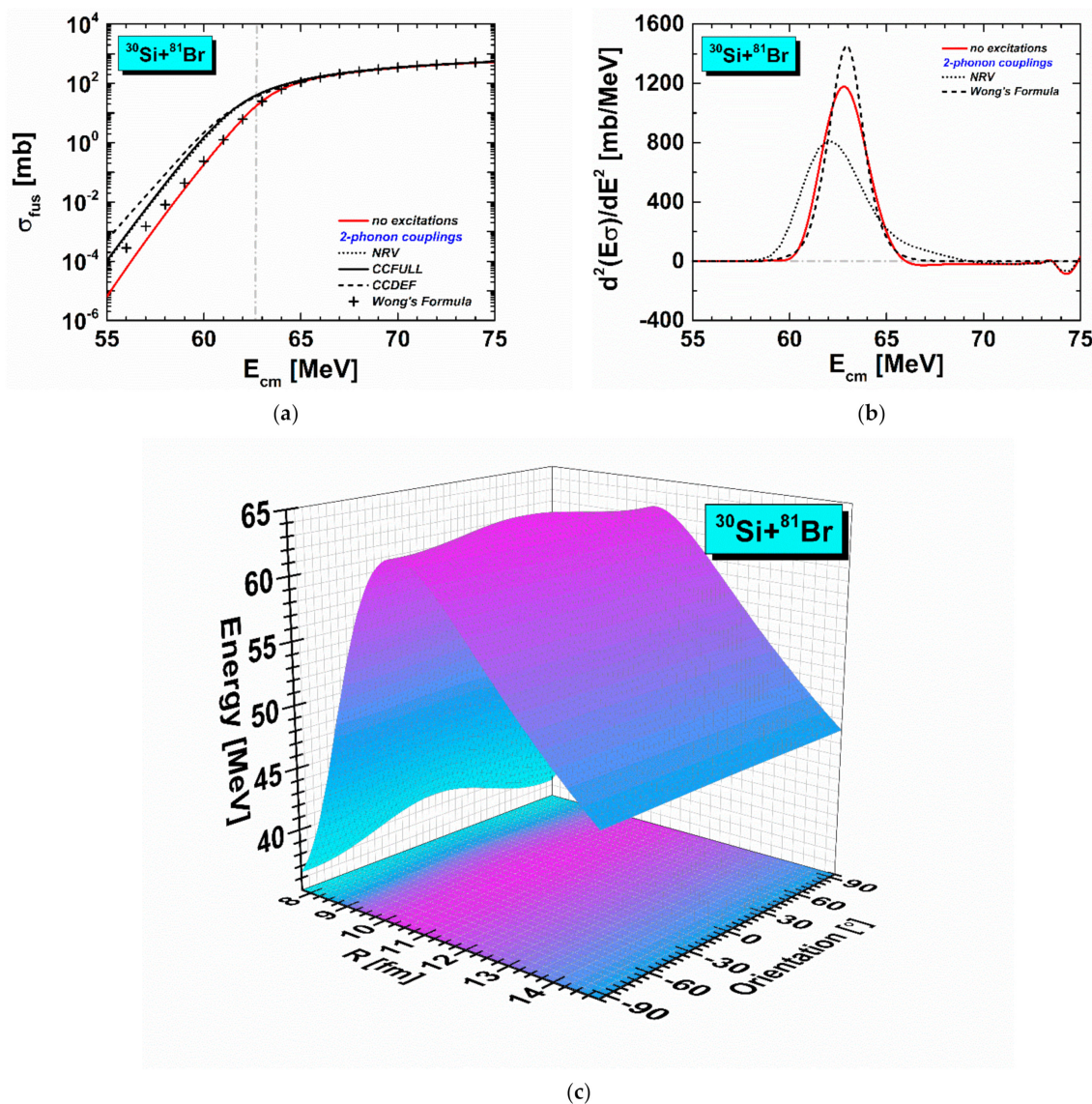


Figure 6. Heavy-ion fusion calculations for $^{30}\text{Si} + ^{81}\text{Br}$ (in the quadrupole and hexadecapole rotational (deformed) state for the ^{30}Si : $E^* = 2.2353$ MeV; $\beta_2 = -0.2360$; $\beta_4 = 0.0400$ and the quadrupole and hexadecapole rotational (deformed) state of the ^{81}Br : $E^* = 0.2760$ MeV; $\beta_2 = 0.1400$; $\beta_4 = -0.0300$ framework) reaction: (a) cross-sections, (b) barrier distributions, and (c) potential energies on mutual orientations in the reactions plane.

In Figure 3b, for the $^{37}\text{Cl} + ^{74}\text{Ge}$ reaction, barrier distribution values change from 0.010 mb/MeV to 19.130 mb/MeV for no excitations calculations; the highest value was observed as 1298 mb/MeV around the barrier. In 2-phonon couplings calculations, barrier distribution values change from 0.011 mb/MeV to 10.990 mb/MeV for NRV; the highest value was observed as 851.7 mb/MeV around the barrier. The barrier distribution values change from 0.009 mb/MeV to 1.245×10^{-6} mb/MeV for Wong's formula calculations; the maximum value was observed as 1380 mb/MeV around the barrier, all values also can be read in the elaboration in Table S7 (this table can be viewed in the Supplementary Information File; Table S7). The calculation outputs that showed good consensus with the experimental outputs were from the 2-phonon couplings in NRV. All calculations are compatible with each other; for this reason, it can be said that the calculations made with the codes used are reliable and consistent.

Fourthly, we analyzed the calculations of the $^{37}\text{Cl} + ^{74}\text{Ge}$ reaction system with NRV, CCFULL, CCDEF codes, and Wong's formula in the energy range of 60–80 MeV with 0.5 MeV steps [22–27]. In Figure 4, the octupole vibrational states for the ^{37}Cl nucleus

has the following parameters [30–35]: $E^* = 4.0100$ MeV; $\beta_{3-} = 0.3300$. The quadrupole and hexadecapole rotational (deformed) states of the ^{74}Ge nucleus has these deformation parameters, respectively [30–35]: $E^* = 0.5959$ MeV; $\beta_2 = -0.2370$; $\beta_4 = -0.0360$. We regulated the potential parameters as follows: $V_0 = 70$ MeV, $r_0 = 1.205$ fm, and $a_0 = 0.670$ fm for all calculations (in Figure 4a–c) [36].

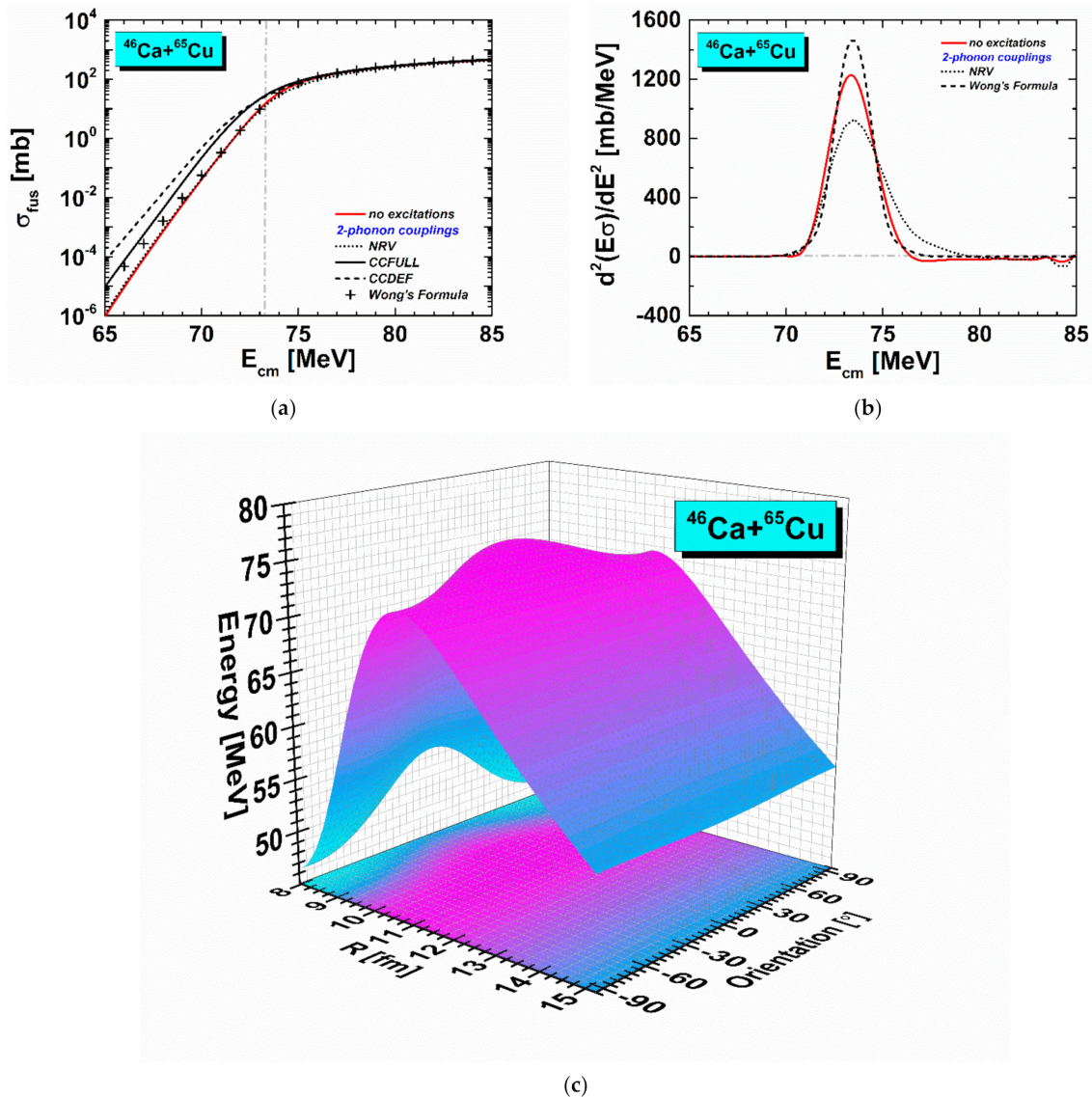


Figure 7. Heavy-ion fusion calculations for $^{46}\text{Ca} + ^{65}\text{Cu}$ (in the quadrupole vibrational state for the ^{46}Ca : $E^* = 1.3460$ MeV; $\beta_{2+} = 0.1468$ and the quadrupole and hexadecapole rotational (deformed) state of the ^{65}Cu : $E^* = 1.4818$ MeV; $\beta_2 = -0.1250$; $\beta_4 = -0.0050$ framework) reaction: (a) cross-sections, (b) barrier distributions, and (c) potential energies on mutual orientations in the reactions plane.

In Figure 4a, for the $^{37}\text{Cl} + ^{74}\text{Ge}$ reaction, cross-section values change from 4.355×10^{-5} mb to 596.8 mb for no excitations calculations. In 2-phonon couplings calculations, values change from 4.071×10^{-5} mb to 542.9 mb for NRV and from 0.002 mb to 623.7 mb for CCFULL, from 0.002 mb to 461.2 mb for CCDEF, and from 4.438×10^{-5} mb to 569.8 mb for Wong's formula; all values also can be read in the elaboration in Table S8 (this table can be viewed in the Supplementary Information File; Table S8). While there are very small differences and negligible distinctions under the barrier region, above the barrier region all calculation codes have once again achieved harmony. The best accordance with the experimental values was monitored in the CCDEF code.

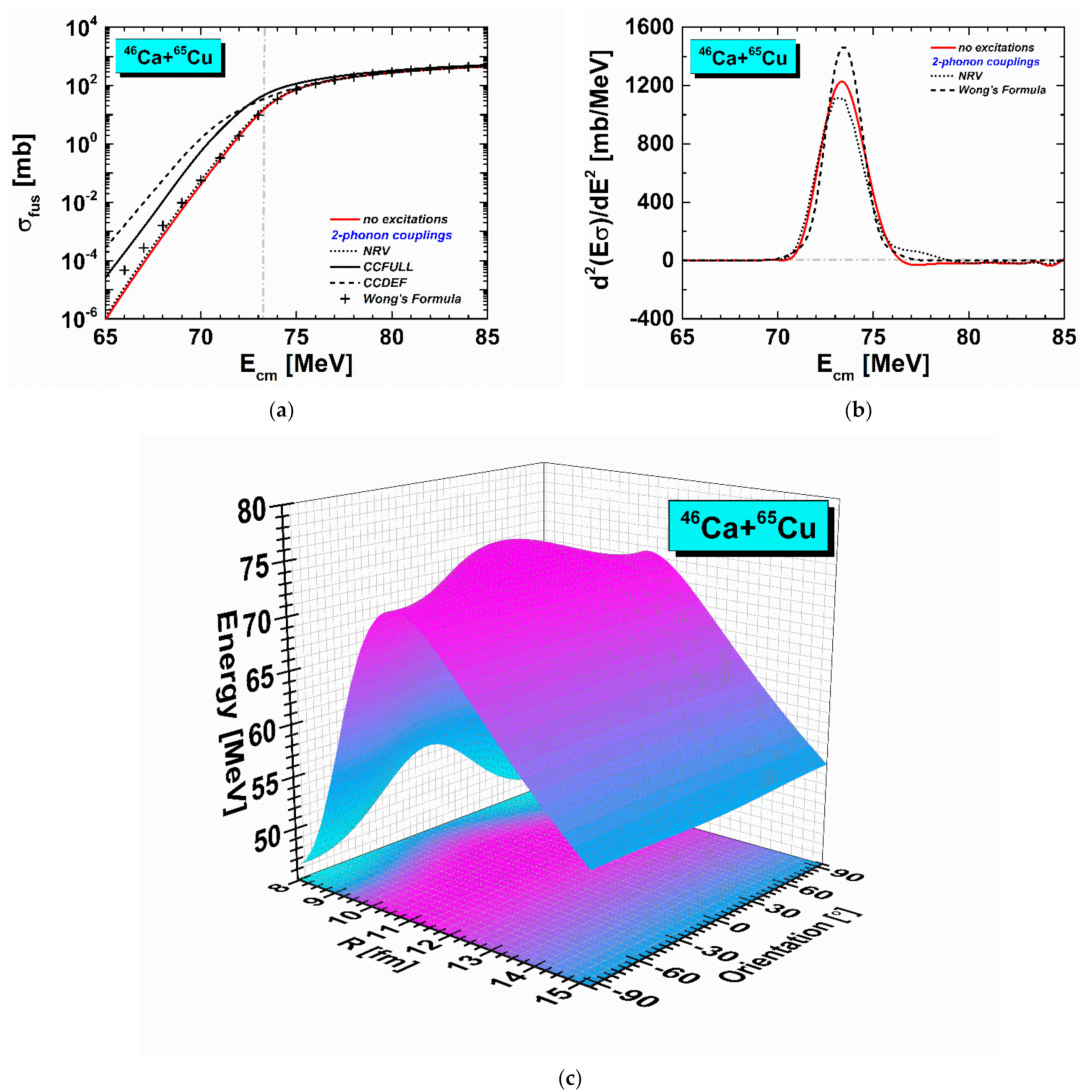


Figure 8. Heavy-ion fusion calculations for $^{46}\text{Ca} + ^{65}\text{Cu}$ (in the octupole vibrational state for the ^{46}Ca : $E^* = 3.6140$ MeV; $\beta_{3-} = 0.2040$ and the quadrupole and hexadecapole rotational (deformed) state of the ^{65}Cu : $E^* = 1.4818$ MeV; $\beta_2 = -0.1250$; $\beta_4 = -0.0050$ framework) reaction: (a) cross-sections, (b) barrier distributions, and (c) potential energies on mutual orientations in the reactions plane.

In Figure 4b, for the $^{37}\text{Cl} + ^{74}\text{Ge}$ reaction, barrier distribution values change from 0.010 mb/MeV to 19.130 mb/MeV for no excitations calculations; the highest value was observed as 1298 mb/MeV around the barrier. In 2-phonon couplings calculations, barrier distribution values change from 0.010 mb/MeV to 46.510 mb/MeV for NRV; the highest value was observed as 880.5 mb/MeV around the barrier. The barrier distribution values change from 0.009 mb/MeV to 1.618×10^{-6} mb/MeV for Wong's formula calculations and the maximum value was observed as 1447 mb/MeV around the barrier; all values also can be read in the elaboration in Table S9 (this table can be viewed in the Supplementary Information File; Table S9).

In Figures 1c, 2c, 3c and 4c, the graphs of the potential energy surface indicate the behavior of the interacting nuclei orientations during fusion. Therefore, the dependence and alterations of the potential energy on the orientations of the nuclei were also investigated for the $^{37}\text{Cl} + ^{74}\text{Ge}$ reaction groups. These dependencies on the R parameter and orientations can be easily analyzed and this figure states that the reaction parameters are highly dependent on the orientation of the interacting nuclei. In accordance with the graphs, the minimum and maximum energy values were observed at the 0° (nose-to-nose interaction) and $\pm 90^\circ$ (side-by-side interaction). The maximum potential

energy value for this reaction is seen around the point contact, that is, around 0° orientation of the interacting nuclei. Some potential energy values at different degrees of orientation of the interacting nuclei can be expressed as follows, with the respective contact points in parentheses: 71.931 MeV ($R = 9.89 \pm 0.05$ fm) for 0° , 69.352 MeV ($R = 10.43 \pm 0.05$ fm) for $\pm 30^\circ$, 66.215 MeV ($R = 11.07 \pm 0.05$ fm) for $\pm 60^\circ$, and 65.527 MeV ($R = 11.29 \pm 0.05$ fm) for $\pm 90^\circ$ in Figure 1c, 72.280 MeV ($R = 9.79 \pm 0.05$ fm) for 0° , 69.713 MeV ($R = 10.32 \pm 0.05$ fm) for $\pm 30^\circ$, 66.564 MeV ($R = 10.96 \pm 0.05$ fm) for $\pm 60^\circ$, and 65.885 MeV ($R = 11.18 \pm 0.05$ fm) for $\pm 90^\circ$ in Figure 2c, 72.601 MeV ($R = 9.79 \pm 0.05$ fm) for 0° , 70.014 MeV ($R = 10.32 \pm 0.05$ fm) for $\pm 30^\circ$, 66.874 MeV ($R = 10.96 \pm 0.05$ fm) for $\pm 60^\circ$, and 66.183 MeV ($R = 11.18 \pm 0.05$ fm) for $\pm 90^\circ$ in Figure 3c, and 72.694 MeV ($R = 9.77 \pm 0.05$ fm) for 0° , 70.108 MeV ($R = 10.30 \pm 0.05$ fm) for $\pm 30^\circ$, 66.958 MeV ($R = 10.94 \pm 0.05$ fm) for $\pm 60^\circ$, and 66.272 MeV ($R = 11.15 \pm 0.05$ fm) for $\pm 90^\circ$ in Figure 4c. When we focus on the position at the saddle point (this point indicates got most important alters), the values at this position tend to change as the angle changes furthermore energies increase towards 0° . The saddle point for the reaction results in Figure 1c is $R = 11.29$ fm and the potential values range from 65.5403 MeV to 67.4950 MeV between $\pm 95^\circ - 0^\circ$. The saddle point for the reaction results in Figure 2c is $R = 11.29$ fm and the potential values range from 65.8705 MeV to 67.5279 MeV between $\pm 95^\circ - 0^\circ$. The saddle point for the reaction results in Figure 3c is $R = 11.29$ fm and the potential values range from 66.1312 MeV to 67.5754 MeV between $\pm 95^\circ - 0^\circ$. The saddle point for the reaction results in Figure 4c is $R = 11.15$ fm and the potential values range from 66.2885 MeV to 68.2685 MeV between $\pm 95^\circ - 0^\circ$. All calculation results can also be read in the elaboration in Table S10 (this table can be viewed in the Supplementary Information File; Table S10). As can be seen from all the results, the change in the deformation parameters also changes the potential between the interacting nuclei.

We can say from our code-based calculations that the influence of vibrational states for the spherical projectile nuclei and rotational states for the deformed target nuclei is the effective couplings leading to big fusion cross-sections around the barrier regions. These four reaction calculations demonstrate that the calculation codes are favorable for all combinations; thus researchers can use any of these as a simulation to investigate the cross-sections, barrier distributions, and potential energy values to acquire a trustworthy output. If the deformation and potential parameters are established meticulously, the outputs that are most appropriate for the experimental data can be acquired via these codes.

3.2. $^{26}\text{Mg} + ^{85}\text{Rb}$, $^{30}\text{Si} + ^{81}\text{Br}$, and $^{46}\text{Ca} + ^{65}\text{Cu}$ Reaction Systems Outputs

Based on our calculation results and observations, to be a reference for new experimental research proposals, fusion cross-sections, barrier distributions, and potential energies on mutual orientations in the reactions plane prospects have been investigated for different reaction channels of ^{111}In radionuclide. Initially, we have handled and determined possible heavy-ion fusion reaction channels with stable projectiles and targets.

In this stage, the production of ^{111}In radionuclide has been analyzed theoretically via fusion reaction of two stable nuclei: $^{26}\text{Mg} + ^{85}\text{Rb}$, $^{30}\text{Si} + ^{81}\text{Br}$, and $^{46}\text{Ca} + ^{65}\text{Cu}$ reactions. We have analyzed, respectively, the $^{26}\text{Mg} + ^{85}\text{Rb}$, $^{30}\text{Si} + ^{81}\text{Br}$, and $^{46}\text{Ca} + ^{65}\text{Cu}$ reactions cross-sections, barrier distributions, and potential energies on mutual orientations in the reactions plane with 0.5 MeV steps in the energy range of 50 – 70 MeV, 55 – 75 MeV, and 65 – 85 MeV (with nuclear states cooperations of the projectile–target nucleus via the CC model). We took the integration parameters as $R_{\text{max}} = 25$ fm and integration step $h = 0.05$ fm in these reaction calculations.

3.2.1. $^{26}\text{Mg} + ^{85}\text{Rb}$ Reaction System Outputs

We analyzed the calculations of the $^{26}\text{Mg} + ^{85}\text{Rb}$ reaction system with NRV, CCFULL, CCDEF codes, and Wong's formula in the energy range of 50–70 MeV with 0.5 MeV steps [22–27]. In Figure 5, the quadrupole and hexadecapole rotational (deformed) states of the ^{26}Mg projectile nucleus has these deformation parameters, respectively [30–35]:

$E^* = 1.8087$ MeV; $\beta_2 = -0.3510$; $\beta_4 = 0.1620$. The quadrupole and hexadecapole rotational (deformed) states of the ^{85}Rb target nucleus has these deformation parameters, respectively [30–35]: $E^* = 0.1512$ MeV; $\beta_2 = 0.0640$; $\beta_4 = -0.0100$. We regulated the potential parameters as follows: $V_0 = 64.073$ MeV, $r_0 = 1.176$ fm, and $a_0 = 0.653$ fm for all calculations (in Figure 5a–c) [36].

In Figure 5a, for the $^{26}\text{Mg} + ^{85}\text{Rb}$ reaction cross-section values change from 2.826×10^{-5} mb to 591.4 mb for no excitations calculations. In 2-phonon couplings calculations, values change from 5.525×10^{-4} mb to 608.6 mb for NRV and from 6.907×10^{-4} mb to 620.7 mb for CCFULL, from 0.004 mb to 604.5 mb for CCDEF, and from 1.953×10^{-4} mb to 618.8 mb for Wong's formula in Table S11 (this table can be viewed in the Supplementary Information File; Table S11). While a perfect match was achieved in NRV, CCFULL, and CCDEF codes in 2-phonon couplings, a negligible difference was observed compared to other calculation methods since the deformation parameters could not be included in Wong's formula.

In Figure 5b, for the $^{26}\text{Mg} + ^{85}\text{Rb}$ reaction barrier distribution values change from 0.005 mb/MeV to 28.660 mb/MeV for no excitations calculations and the highest value was observed as 1154 mb/MeV around the barrier. In 2-phonon couplings calculations, barrier distribution values change from 0.066 mb/MeV to 28.920 mb/MeV for NRV and the highest value was observed as 870.0 mb/MeV around the barrier. The barrier distribution values change from 0.028 mb/MeV to 2.818×10^{-6} mb/MeV for Wong's formula calculations and the maximum value was observed as 1361 mb/MeV around the barrier in Table S12 (this table can be viewed in the Supplementary Information File; Table S12). As can be seen in the NRV calculation, the number of channels and the potential parameter can be increased to eliminate the small extra peaks that appear after passing the general peak regions.

As can be observed in Figure 5c, the reaction parameters are highly dependent on the orientation of the interacting nuclei. In accordance with this figure, the minimum and maximum energy values were generally observed at the 0° (nose-to-nose interaction) and $\pm 90^\circ$ (side-by-side interaction). The minimum potential energy value for this reaction is seen around the point contact, that is, around 0° orientation of the interacting nuclei. Some potential energy values at different degrees of orientation of the interacting nuclei can be expressed as follows, with the respective contact points in parentheses: 58.087 MeV ($R = 10.16 \pm 0.05$ fm) for 0° , 59.582 MeV ($R = 9.95 \pm 0.05$ fm) for $\pm 30^\circ$, 58.146 MeV ($R = 10.26 \pm 0.05$ fm) for $\pm 60^\circ$, and 55.620 MeV ($R = 10.77 \pm 0.05$ fm) for $\pm 90^\circ$. The saddle point for the reaction results in Figure 5c is $R = 10.77$ fm and the potential values range from 55.7097 MeV to 57.1413 MeV between $\pm 95^\circ - 0^\circ$. All calculation results can also be read in the elaboration in Table S10 (this table can be viewed in the Supplementary Information File; Table S10). Since this reaction represents the interaction of two deformed nuclei, there are two peaks where the maximum value is observed, and these peak points are approximately at the $\pm 41.8^\circ$ positions.

3.2.2. $^{30}\text{Si} + ^{81}\text{Br}$ Reaction System Outputs

In Figure 6, we analyzed the calculations of the $^{30}\text{Si} + ^{81}\text{Br}$ reaction system with NRV, CCFULL, CCDEF codes, and Wong's formula in the energy range of 55–75 MeV with 0.5 MeV steps [22–27]. The quadrupole and hexadecapole rotational (deformed) states of the ^{30}Si projectile nucleus has these deformation parameters respectively [30–35]: $E^* = 2.2353$ MeV; $\beta_2 = -0.2360$; $\beta_4 = 0.0400$. The quadrupole and hexadecapole rotational (deformed) states of the ^{81}Br target nucleus has these deformation parameters, respectively [30–35]: $E^* = 0.2760$ MeV; $\beta_2 = 0.1400$; $\beta_4 = -0.0300$. We regulated the potential parameters as follows: $V_0 = 65.947$ MeV, $r_0 = 1.176$ fm, and $a_0 = 0.661$ fm for all calculations (in Figure 6a–c) [36].

In Figure 6a, for $^{30}\text{Si} + ^{81}\text{Br}$ reaction cross-section values change from 6.389×10^{-6} mb to 529.7 mb for no excitations calculations. In 2-phonon couplings calculations, values change from 8.787×10^{-5} mb to 540.0 mb for NRV and from 1.049×10^{-4} mb to 547.9 mb for CCFULL, from 5.276×10^{-4} mb to 539.4 mb for CCDEF, and from 5.227×10^{-5} mb to

553.8 mb for Wong's formula in Table S13 (this table can be viewed in the Supplementary Information File; Table S13). Since the deformation parameters cannot be included in Wong's formula calculations, its behavior here shows similar characteristics to the no excitations. On the other hand, since all codes take into account deformation parameters, they are compatible with each other in a common attitude.

In Figure 6b, for $^{30}\text{Si} + ^{81}\text{Br}$ reaction barrier distribution values change from 0.001 mb/MeV to 32.550 mb/MeV for no excitations calculations and the highest value was observed as 1163 mb/MeV around the barrier. In 2-phonon couplings calculations, barrier distribution values change from 0.014 mb/MeV to 32.640 mb/MeV for NRV and the highest value was observed as 817.1 mb/MeV around the barrier. The barrier distribution values change from 0.008 mb/MeV to 6.775×10^{-6} mb/MeV for Wong's formula calculations and the maximum value was observed as 1453 mb/MeV around the barrier in Table S14 (this table can be viewed in the Supplementary Information File; Table S14). The fact that two calculation codes peak at almost the same point indicates that the results are reliable.

In accordance with Figure 6c, the minimum and maximum energy values were observed at the 0° (nose-to-nose interaction) and $\pm 90^\circ$ (side-by-side interaction). The maximum potential energy value for this reaction is seen around the point contact, that is, around 0° orientation of the interacting nuclei. Some potential energy values at different degrees of orientation of the interacting nuclei can be expressed as follows, with the respective contact points in parentheses: 63.827 MeV ($R = 10.34 \pm 0.05$ fm) for 0° , 63.535 MeV ($R = 10.34 \pm 0.05$ fm) for $\pm 30^\circ$, 62.985 MeV ($R = 10.44 \pm 0.05$ fm) for $\pm 60^\circ$, and 62.738 MeV ($R = 10.44 \pm 0.05$ fm) for $\pm 90^\circ$ in Figure 6c. The saddle point for the reaction results in Figure 6c is $R = 10.44$ fm and the potential values range from 62.7453 MeV to 63.7654 MeV between $\pm 95^\circ - 0^\circ$. These results also can be read in the elaboration in Table S10 (this table can be viewed in the Supplementary Information File; Table S10).

3.2.3. $^{46}\text{Ca} + ^{65}\text{Cu}$ Reaction System Outputs

In the last reaction proposal, we analyzed the calculations of the $^{46}\text{Ca} + ^{65}\text{Cu}$ reaction system with NRV, CCFULL, CCDEF codes, and Wong's Formula in the energy range of 65–85 MeV with 0.5 MeV steps [22–27]. In Figure 7, the quadrupole vibrational states for the ^{46}Ca nucleus has the following parameters [30–35]: $E^* = 1.3460$ MeV; $\beta_{2+} = 0.1468$. The quadrupole and hexadecapole rotational (deformed) states of the ^{65}Cu nucleus has these deformation parameters respectively [30–35]: $E^* = 1.4818$ MeV; $\beta_2 = -0.1250$; $\beta_4 = -0.0050$. We regulated the potential parameters as follows: $V_0 = 69.273$ MeV, $r_0 = 1.176$ fm, and $a_0 = 0.668$ fm for all calculations (in Figure 7a–c) [36].

In Figure 7a, for $^{46}\text{Ca} + ^{65}\text{Cu}$ reaction cross-section values change from 9.247×10^{-7} mb to 456.2 mb for no excitations calculations. In 2-phonon couplings calculations, values change from 1.144×10^{-6} mb to 426.2 mb for NRV and from 9.342×10^{-6} mb to 472.6 mb for CCFULL, from 7.083×10^{-5} mb to 468.8 mb for CCDEF, and from 7.938×10^{-6} mb to 477.7 mb for Wong's formula in Table S15 (this table can be viewed in the Supplementary Information File; Table S15).

In Figure 7b, for the $^{46}\text{Ca} + ^{65}\text{Cu}$ reaction, barrier distribution values change from 1.902×10^{-4} mb/MeV to 12.770 mb/MeV for no excitations calculations and the highest value was observed as 1219 mb/MeV around the barrier. In 2-phonon couplings calculations, barrier distribution values change from 2.387×10^{-4} mb/MeV to 31.480 mb/MeV for NRV and the highest value was observed as 930.5 mb/MeV around the barrier. The barrier distribution values change from 0.002 mb/MeV to 6.922×10^{-6} mb/MeV for Wong's formula calculations and the maximum value was observed as 1327 mb/MeV around the barrier in Table S16 (this table can be viewed in the Supplementary Information File; Table S16).

In Figure 8, we analyzed the calculations of the $^{46}\text{Ca} + ^{65}\text{Cu}$ reaction system with NRV, CCFULL, CCDEF codes, and Wong's formula in the energy range of 65–85 MeV with 0.5 MeV steps [22–27]. The octupole vibrational states for the ^{46}Ca nucleus has the following parameters [30–35]: $E^* = 3.6140$ MeV; $\beta_{3-} = 0.2040$. The quadrupole and

hexadecapole rotational (deformed) states of the ^{65}Cu nucleus has these deformation parameters respectively [30–35]: $E^* = 1.4818$ MeV; $\beta_2 = -0.1250$; $\beta_4 = -0.0050$. We regulated the potential parameters as follows: $V_0 = 69.273$ MeV, $r_0 = 1.176$ fm, and $a_0 = 0.668$ fm for all calculations (in Figure 8a–c) [36].

In Figure 8a, for $^{46}\text{Ca} + ^{65}\text{Cu}$ reaction cross-section values change from 9.247×10^{-7} mb to 456.2 mb for no excitations calculations. In 2-phonon couplings calculations, values change from 1.190×10^{-6} mb to 449.6 mb for NRV and from 2.610×10^{-5} mb to 511.4 mb for CCFULL, from 2.720×10^{-4} mb to 471.7 mb for CCDEF, and from 7.938×10^{-6} mb to 477.7 mb for Wong's formula in Table S17 (this table can be viewed in the Supplementary Information File; Table S17).

In Figure 8b, for $^{46}\text{Ca} + ^{65}\text{Cu}$ reaction barrier distribution values change from 1.902×10^{-4} mb/MeV to 12.770 mb/MeV for no excitations calculations and the highest value was observed as 1219 mb/MeV around the barrier. In 2-phonon couplings calculations, barrier distribution values change from 2.481×10^{-4} mb/MeV to 8.328 mb/MeV for NRV and the highest value was observed as 1117 mb/MeV around the barrier. The barrier distribution values change from 0.002 mb/MeV to 6.922×10^{-6} mb/MeV for Wong's Formula calculations and the maximum value was observed as 1327 mb/MeV around the barrier in Table S18 (this table can be viewed in the Supplementary Information File; Table S18). The fact that two calculation codes peak at almost the same point indicates that the results are reliable for the barrier distribution function.

In Figures 7c and 8c, the graph of the potential energy surface indicates the behavior of the interacting nuclei' orientations during fusion. Therefore, the dependence and alterations of the potential energy on the orientations of the nuclei were also investigated for $^{46}\text{Ca} + ^{65}\text{Cu}$ reaction groups. With Figure 8c, this dependence on the R parameter and orientations can be easily analyzed and these figures state that the reaction parameters are largely related to the orientation of the interacting nuclei. The minimum and maximum energy values were observed at the 0° (nose-to-nose interaction) and $\pm 90^\circ$ (side-by-side interaction). The maximum potential energy value for this reaction is seen around the point contact, that is, around 0° orientation of the interacting nuclei. Some potential energy values at different degrees of orientation of the interacting nuclei can be expressed as follows, with the respective contact points in parentheses: 75.711 MeV ($R = 10.12 \pm 0.05$ fm) for 0° , 74.761 MeV ($R = 10.33 \pm 0.05$ fm) for $\pm 30^\circ$, 73.154 MeV ($R = 10.64 \pm 0.05$ fm) for $\pm 60^\circ$, and 72.516 MeV ($R = 10.75 \pm 0.05$ fm) for $\pm 90^\circ$ in Figure 7c and 75.711 MeV ($R = 10.12 \pm 0.05$ fm) for 0° , 74.761 MeV ($R = 10.33 \pm 0.05$ fm) for $\pm 30^\circ$, 73.154 MeV ($R = 10.64 \pm 0.05$ fm) for $\pm 60^\circ$, and 72.516 MeV ($R = 10.75 \pm 0.05$ fm) for $\pm 90^\circ$ in Figure 8c. The saddle point for the reaction results in Figure 7c is $R = 10.75$ fm and in Figure 8c is $R = 10.75$ fm. The potential energy values range from 72.5203 MeV to 74.1668 MeV for Figure 7c and from 72.5346 MeV to 74.5466 MeV for Figure 8c calculations between $\pm 95^\circ$ – 0° , respectively. All computation outputs can also be viewed in Table S10 (this table can be viewed in the Supplementary Information File; Table S10). As can be observed from all the computations, the alterations in the deformation parameters also vary the potential among the interacting nuclei.

If we interpret all of the computation outputs and their graphs in general from the theoretical perspective, the interaction of nuclei with each other is highly dependent on their deformation parameters and their spatial orientations during the interaction. The attractive forces acting at short distances depend on the distance between the surfaces of the interacting nuclei, but the repulsive forces acting at large distances depend on the distance R between the centers of the nuclei. For example, as can be seen from our three-dimensional (3D) potential energies on mutual orientations in the reactions plane graphs, if we consider the moments when two interacting nuclei touch each other, the nuclear forces remain constant at this zero point, and meanwhile, the Coulomb energy decreases as significantly as the distance between the nuclei to which it is connected. As the distance between the core centers begins to increase, the potential energy begins to decrease. A well-rounded portrayal of the potential energies of the interactions, as well as equations

and reaction kinematics for its computation method, can be found in [1,24] and in the NRV official webpage (<http://nrv.jinr.ru/nrv>) (accessed on 12 December 2021).

Our theoretical wide-scaled outputs show that all codes are realistic if the parameters are calculated carefully, so they can be used as a simulation to obtain the cross-section values to get a reliable idea.

4. Conclusions

This theoretical analysis-based investigation exhibits the importance of heavy-ion fusion reaction calculations maintained via stable projectile and target nuclei and the noteworthy of a way to comprehend the chief influence of the target-projectile couplings in radionuclide research.

In this research, firstly, we have explored the $^{37}\text{Cl} + ^{74}\text{Ge}$ reaction cross-sections and barrier distributions crosschecked with experimental outputs at 0.5 MeV steps in the energy area of 60–80 MeV (via different calculation codes and deformation parameter compositions of the projectile–target nuclei in the CC code). Our calculating outcomes are in a harmony with the experimental data. Then, based on these results, we have proposed three different reactions where we theoretically calculate fusion cross-sections and barrier distributions with different codes and nuclear parameter combinations, which experimental outputs are not existing in the published works: $^{26}\text{Mg} + ^{85}\text{Rb}$, $^{30}\text{Si} + ^{81}\text{Br}$, and $^{46}\text{Ca} + ^{65}\text{Cu}$ reactions.

The calculation methods we used are practical, simple, understandable, and modernist methods to achieve and stiffen dexterities in complying with coeval approaches to characterize the characteristics of nuclei and to be able to view the parameters of nuclear collisions; in addition, they can be blended with experimental data. Benchmarking of the outputs of comprehensive calculations based on the CC model with experimental data has facilitated our interpretation of the effect of deformation parameters and the importance of calculation codes in the heavy-ion fusion process.

We concluded that CC and phonon excitation influences augment the calculated cross-sections at energies near the barrier district. It is observed that the influence of vibrational states for the spherical nuclei and rotational states for the deformed nuclei, is the effective couplings leading to big fusion cross-sections around the barrier regions. As can be seen in the calculations, despite there being very minor distinctions bottom the barrier zone, computations ordinarily arrived in obvious harmony with one another supra the barrier zone. All calculating outcomes, codes, and parameters are in exquisite compatibility with each other in the calculation model. In accordance with the purpose of the study, the reactions were studied with NRV, CCFULL, CCDEF, and Wong's formula; it was shown with the obtained results that, although the mathematical (numerical) realizations in the calculation codes were different in some details, the algorithm is close to the same at a level close to the total. The CC model describes all of the experimental data well and also produces compatible fusion cross-section alterations. The alterations of the fusion cross-sections at sub ($E < V_C$), near ($E \approx V_C$), and above ($E > V_C$) barrier according to the energy values are frankly observed with the help of the data in Figure 1. It can also be seen in our theoretical calculations that at energies above the barrier, the cross-section is harmonious with one another in just about all computing methods collaborations, while minor distinctions or secessions are inhabited for cross-sections at the sub-barrier region. The outcome that the behavior of the cross-sections is fully designated by the deformation coefficients has been approved by many explorers with various works.

The rotations in heavier targets are more powerful and their effects on the fusion process of the associated interaction may not be disregarded and hence is expected to be more grand. Investigating some deflections between these estimations and sub-barrier fusion outputs is important for the development of fusion reaction studies below barrier regions. Furthermore, the impacts of coupled channels on the fusion reaction are crucial. Such influences are observed to ascend as one moves from a stable target nucleus with a small number of neutrons to a stable target nucleus with a large number of neutrons.

In terms of guiding future studies: more mixed and dissimilar potential models can be utilized to further cultivate reaction computations and research can be strengthened via new codes and simulations. In this way, by constituting the most suitable infrastructure for experimental studies, we can provide a trustworthy datum by using these infrastructures and information in cases where experimental systems are impossible.

Supplementary Materials: The following are available online at <https://www.mdpi.com/article/10.3390/en14248594/s1>, Table S1. Abbreviation and symbols of coupled channel (CC) model section in the main text, Table S2. Heavy-ion fusion cross-section calculations for $^{37}\text{Cl} + ^{74}\text{Ge}$ (in the quadrupole vibrational state for the ^{37}Cl : $E^* = 1.7266$ MeV; $\beta_{2+} = 0.1400$ and the quadrupole and hexadecapole rotational (deformed) state of the ^{74}Ge : $E^* = 0.5959$ MeV; $\beta_2 = -0.2370$; $\beta_4 = -0.0360$ framework) reaction, Table S3. Heavy-ion fusion barrier-distributions calculations for $^{37}\text{Cl} + ^{74}\text{Ge}$ (in the quadrupole vibrational state for the ^{37}Cl : $E^* = 1.7266$ MeV; $\beta_{2+} = 0.1400$ and the quadrupole and hexadecapole rotational (deformed) state of the ^{74}Ge : $E^* = 0.5959$ MeV; $\beta_2 = -0.2370$; $\beta_4 = -0.0360$ framework) reaction, Table S4. Heavy-ion fusion cross-section calculations for $^{37}\text{Cl} + ^{74}\text{Ge}$ (in the quadrupole vibrational state for the ^{37}Cl : $E^* = 3.0861$ MeV; $\beta_{2+} = 0.2400$ and the quadrupole and hexadecapole rotational (deformed) state of the ^{74}Ge : $E^* = 0.5959$ MeV; $\beta_2 = -0.2370$; $\beta_4 = -0.0360$ framework) reaction, Table S5. Heavy-ion fusion barrier-distributions calculations for $^{37}\text{Cl} + ^{74}\text{Ge}$ (in the quadrupole vibrational state for the ^{37}Cl : $E^* = 3.0861$ MeV; $\beta_{2+} = 0.2400$ and the quadrupole and hexadecapole rotational (deformed) state of the ^{74}Ge : $E^* = 0.5959$ MeV; $\beta_2 = -0.2370$; $\beta_4 = -0.0360$ framework) reaction, Table S6. Heavy-ion fusion cross-section calculations for $^{37}\text{Cl} + ^{74}\text{Ge}$ (in the octupole vibrational state for the ^{37}Cl : $E^* = 3.1035$ MeV; $\beta_{3-} = 0.3200$ and the quadrupole and hexadecapole rotational (deformed) state of the ^{74}Ge : $E^* = 0.5959$ MeV; $\beta_2 = -0.2370$; $\beta_4 = -0.0360$ framework) reaction, Table S7. Heavy-ion fusion barrier-distributions calculations for $^{37}\text{Cl} + ^{74}\text{Ge}$ (in the octupole vibrational state for the ^{37}Cl : $E^* = 3.1035$ MeV; $\beta_{3-} = 0.3200$ and the quadrupole and hexadecapole rotational (deformed) state of the ^{74}Ge : $E^* = 0.5959$ MeV; $\beta_2 = -0.2370$; $\beta_4 = -0.0360$ framework) reaction, Table S8. Heavy-ion fusion cross-section calculations for $^{37}\text{Cl} + ^{74}\text{Ge}$ (in the octupole vibrational state for the ^{37}Cl : $E^* = 4.0100$ MeV; $\beta_{3-} = 0.3300$ and the quadrupole and hexadecapole rotational (deformed) state of the ^{74}Ge : $E^* = 0.5959$ MeV; $\beta_2 = -0.2370$; $\beta_4 = -0.0360$ framework) reaction, Table S9. Heavy-ion fusion barrier-distributions calculations for $^{37}\text{Cl} + ^{74}\text{Ge}$ (in the octupole vibrational state for the ^{37}Cl : $E^* = 4.0100$ MeV; $\beta_{3-} = 0.3300$ and the quadrupole and hexadecapole rotational (deformed) state of the ^{74}Ge : $E^* = 0.5959$ MeV; $\beta_2 = -0.2370$; $\beta_4 = -0.0360$ framework) reaction, Table S10. Heavy-ion fusion potential energies on mutual orientations in the reactions plane calculations for $^{37}\text{Cl} + ^{74}\text{Ge}$, $^{26}\text{Mg} + ^{85}\text{Rb}$, $^{30}\text{Si} + ^{81}\text{Br}$, and $^{46}\text{Ca} + ^{65}\text{Cu}$ reactions, Table S11. Heavy-ion fusion cross-section calculations for $^{26}\text{Mg} + ^{85}\text{Rb}$ (in the quadrupole and hexadecapole rotational (deformed) state for the ^{26}Mg : $E^* = 1.8087$ MeV; $\beta_2 = -0.3510$; $\beta_4 = 0.1620$ and the quadrupole and hexadecapole rotational (deformed) state of the ^{85}Rb : $E^* = 0.1512$ MeV; $\beta_2 = 0.0640$; $\beta_4 = -0.0100$ framework) reaction, Table S12. Heavy-ion fusion barrier-distributions calculations for $^{26}\text{Mg} + ^{85}\text{Rb}$ (in the quadrupole and hexadecapole rotational (deformed) state for the ^{26}Mg : $E^* = 1.8087$ MeV; $\beta_2 = -0.3510$; $\beta_4 = 0.1620$ and the quadrupole and hexadecapole rotational (deformed) state of the ^{85}Rb : $E^* = 0.1512$ MeV; $\beta_2 = 0.0640$; $\beta_4 = -0.0100$ framework) reaction, Table S13. Heavy-ion fusion cross-section calculations for $^{30}\text{Si} + ^{81}\text{Br}$ (in the quadrupole and hexadecapole rotational (deformed) state for the ^{30}Si : $E^* = 2.2353$ MeV; $\beta_2 = -0.2360$; $\beta_4 = 0.0400$ and the quadrupole and hexadecapole rotational (deformed) state of the ^{81}Br : $E^* = 0.2760$ MeV; $\beta_2 = 0.1400$; $\beta_4 = -0.0300$ framework) reaction, Table S14. Heavy-ion fusion barrier-distributions calculations for $^{30}\text{Si} + ^{81}\text{Br}$ (in the quadrupole and hexadecapole rotational (deformed) state for the ^{30}Si : $E^* = 2.2353$ MeV; $\beta_2 = -0.2360$; $\beta_4 = 0.0400$ and the quadrupole and hexadecapole rotational (deformed) state of the ^{81}Br : $E^* = 0.2760$ MeV; $\beta_2 = 0.1400$; $\beta_4 = -0.0300$ framework) reaction, Table S15. Heavy-ion fusion cross-section calculations for $^{46}\text{Ca} + ^{65}\text{Cu}$ (in the quadrupole vibrational state for the ^{46}Ca : $E^* = 1.3460$ MeV; $\beta_{2+} = 0.1468$ and the quadrupole and hexadecapole rotational (deformed) state of the ^{65}Cu : $E^* = 1.4818$ MeV; $\beta_2 = -0.1250$; $\beta_4 = -0.0050$ framework) reaction, Table S16. Heavy-ion fusion barrier-distributions calculations for $^{46}\text{Ca} + ^{65}\text{Cu}$ (in the quadrupole vibrational state for the ^{46}Ca : $E^* = 1.3460$ MeV; $\beta_{2+} = 0.1468$ and the quadrupole and hexadecapole rotational (deformed) state of the ^{65}Cu : $E^* = 1.4818$ MeV; $\beta_2 = -0.1250$; $\beta_4 = -0.0050$ framework) reaction, Table S17. Heavy-ion fusion cross-section calculations for $^{46}\text{Ca} + ^{65}\text{Cu}$ (in the octupole vibrational state for the ^{46}Ca : $E^* = 3.6140$ MeV; $\beta_{3-} = 0.2040$ and the quadrupole and hexadecapole rotational (deformed) state of the ^{65}Cu : $E^* = 1.4818$ MeV; $\beta_2 =$

−0.1250; $\beta_4 = -0.0050$ framework) reaction, Table S18. Heavy-ion fusion barrier-distributions calculations for $^{46}\text{Ca} + ^{65}\text{Cu}$ (in the octupole vibrational state for the ^{46}Ca : $E^* = 3.6140$ MeV; $\beta_{3-} = 0.2040$ and the quadrupole and hexadecapole rotational (deformed) state of the ^{65}Cu : $E^* = 1.4818$ MeV; $\beta_2 = -0.1250$; $\beta_4 = -0.0050$ framework) reaction.

Author Contributions: Z.M.C.: Conceptualization, methodology, software, validation, investigation, resources, CC code analysis, NRV-CCFULL-Wong’s calculation, writing—original draft preparation, review and editing, visualization, supervision. B.E.: CCDEF calculation and review. T.B.: Review. A.H.Y.: Conceptualization, methodology, validation, review, editing, and supervision. All authors have read and agreed to the published version of the manuscript.

Funding: This research received no external funding.

Institutional Review Board Statement: Not applicable.

Informed Consent Statement: Not applicable.

Data Availability Statement: The data presented in this study are available on request from the corresponding author.

Conflicts of Interest: The authors declare no conflict of interest.

References

- Zagrebaev, V. *Heavy Ion. Reactions at Low Energies*; Springer: Singapore, 2019; pp. 99–144.
- Lépine-Szily, A.; Lichtenthäler, R. Coupled channels effects in heavy ion reactions. *Eur. Phys. J. A* **2021**, *57*, 99. [[CrossRef](#)]
- Deb, N.K.; Kalita, K.; Al Rashid, H.; Nath, S.; Gehlot, J.; Madhavan, N.; Biswas, R.; Sahoo, R.N.; Giri, P.K.; Das, A.; et al. Role of neutron transfer in the sub-barrier fusion cross section in $^{18}\text{O} + ^{116}\text{Sn}$. *Phys. Rev. C* **2020**, *102*, 034603. [[CrossRef](#)]
- Gharaei, R.; Hasanzade, H. Sub-barrier fusion of $^{34,36}\text{S} + ^{204,206,208}\text{Pb}$: Signature of isotopic dependence of repulsive core potential in heavy-ion fusion reactions. *Nucl. Phys. A* **2021**, *1013*, 122223. [[CrossRef](#)]
- Stefanini, A.M.; Montagnoli, G.; D’Andrea, M.; Giacomini, M.; Dehman, C.; Somasundaram, R.; Vijayan, V.; Zago, L.; Colucci, G.; Galtarossa, F.; et al. New insights into sub-barrier fusion of $^{28}\text{Si} + ^{100}\text{Mo}$. *J. Phys. G Nucl. Part. Phys.* **2021**, *48*, 055101. [[CrossRef](#)]
- Vijay, C.; Chahal, R.P.; Gautam, M.S.; Duhan, S.; Khatri, H. Fusion cross sections and barrier distributions for $\text{O}^{16} + \text{Ge}^{70,72,73,74,76}$ and $\text{O}^{18} + \text{Ge}^{74}$ reactions at energies near and below the Coulomb barrier. *Phys. Rev. C* **2021**, *103*, 024607. [[CrossRef](#)]
- Baby, L.T.; Tripathi, V.; Das, J.J.; Sugathan, P.; Madhavan, N.; Sinha, A.K.; Radhakrishna, M.C.; Rao, P.V.M.; Hui, S.K.; Hagino, K. Role of 28Si excitations in the sub-barrier fusion of $^{28}\text{Si} + ^{120}\text{Sn}$. *Phys. Rev. C* **2000**, *62*, 014603. [[CrossRef](#)]
- Wilkinson, J.T.; Barrett, K.E.; Ferran, S.J.; McGuinness, S.R.; McIntosh, L.A.; McCarthy, M.; Yennello, S.J.; Engle, J.W.; Lapi, S.E.; Peaslee, G.F. A heavy-ion production channel of ^{149}Tb via ^{63}Cu bombardment of ^{89}Y . *Appl. Radiat. Isot.* **2021**, *178*, 109935. [[CrossRef](#)]
- McGuinness, S.R.; Wilkinson, J.T.; Peaslee, G.F. Heavy-ion production of ^{77}Br and ^{76}Br . *Sci. Rep.* **2021**, *11*, 15749. [[CrossRef](#)]
- Colucci, G.; Montagnoli, G.; Stefanini, A.M.; Hagino, K.; Cacioli, A.; Čolović, P.; Corradi, L.; Fioretto, E.; Galtarossa, F.; Goasduff, A.; et al. Study of sub-barrier fusion of $^{36}\text{S} + ^{50}\text{Ti}, ^{51}\text{V}$ systems. *EPJ Web Conf.* **2019**, *223*, 01013. [[CrossRef](#)]
- Erol, B.; Cinan, Z.; Baskan, T.; Yilmaz, A. Investigating medium and heavy mass heavy-ion fusion reactions and barrier distributions with coupled-channel analyzes. *Acta Phys. Pol. B* **2021**, *52*, 1117. [[CrossRef](#)]
- Mei, B.; Balabanski, D.L.; Hua, W.; Zhang, Y.-H.; Zhou, X.-H.; Yuan, C.-X.; Su, J. Fusion reactions around the barrier for $\text{Be} + ^{238}\text{U}$. *Chin. Phys. C* **2021**, *45*, 054001. [[CrossRef](#)]
- Mohammadi, J.; Ghodsi, O.N. Study of the dinuclear system for $^{296}119$ superheavy compound nucleus in fusion reactions. *Chin. Phys. C* **2021**, *45*, 044107. [[CrossRef](#)]
- Asher, B.W.; Almaraz-Calderon, S.; Tripathi, V.; Kemper, K.W.; Baby, L.T.; Gerken, N.; Lopez-Saavedra, E.; Morelock, A.B.; Perello, J.F.; Wiedenhöver, I.; et al. Experimental study of the $\text{F}^{17} + \text{C}^{12}$ fusion reaction and its implications for fusion of proton-halo systems. *Phys. Rev. C* **2021**, *103*, 044615. [[CrossRef](#)]
- Gautam, M.S.; Vinod, K.; Kumar, H. Role of barrier modification and nuclear structure effects in sub-barrier fusion dynamics of various heavy ion fusion reactions. *Braz. J. Phys.* **2017**, *47*, 461–472. [[CrossRef](#)]
- Jiang, C.L.; Back, B.B.; Rehm, K.E.; Hagino, K.; Montagnoli, G.; Stefanini, A.M. Heavy-ion fusion reactions at extreme sub-barrier energies. *Eur. Phys. J. A* **2021**, *57*, 235. [[CrossRef](#)]
- Abd Madhi, M.H.; Majeed, F.A. Fusion reaction study of halo system by quantum mechanical-based model for $^6\text{He} + ^{64}\text{Zn}$, $^8\text{B} + ^{58}\text{Ni}$ and $^8\text{He} + ^{197}\text{Au}$ systems. *Bull. Pol. Acad. Sci. Tech. Sci.* **2021**, *69*, 4. [[CrossRef](#)]
- Rong, C.H.; Rangel, J.; Wu, Y.S.; Zhang, G.L.; Lin, C.J.; Cardozo, E.N.; Wang, X.Y.; Yang, L.; Ma, N.R.; Wang, D.X.; et al. Study of quasi-elastic scattering of $^{17}\text{F} + ^{208}\text{Pb}$ and $^{17}\text{F} + ^{208}\text{Pb}$ at energies around Coulomb barrier. *Eur. Phys. J. A* **2021**, *57*, 1–18. [[CrossRef](#)]
- Zagrebaev, V.I.; Aritomo, Y.; Itkis, M.G.; Oganessian, Y.T.; Ohta, M. Synthesis of superheavy nuclei: How accurately can we describe it and calculate the cross sections? *Phys. Rev. C* **2001**, *65*, 014607. [[CrossRef](#)]
- Rowley, N.; Satchler, G.; Stelson, P. On the “distribution of barriers” interpretation of heavy-ion fusion. *Phys. Lett. B* **1991**, *254*, 25–29. [[CrossRef](#)]

21. Rowley, N. Sub-barrier fusion: Probing reaction dynamics with barrier distributions. *Nucl. Phys. A* **1992**, *538*, 205–220. [[CrossRef](#)]
22. Hagino, K.; Rowley, N.; Kruppa, A. A program for coupled-channel calculations with all order couplings for heavy-ion fusion reactions. *Comput. Phys. Commun.* **1999**, *123*, 143–152. [[CrossRef](#)]
23. Zagrebaev, V.I.; Samarin, V.V. Near-barrier fusion of heavy nuclei: Coupling of channels. *Phys. At. Nucl.* **2004**, *67*, 1462–1477. [[CrossRef](#)]
24. Zagrebaev, V.I.; Kozhin, A. Nuclear reactions video (knowledge base on low energy nuclear physics). *JINR Rep.* **1999**, *E10*, 99–151.
25. Fernández-Niello, J.; Dasso, C.H.; Landowne, S. CCDEF—A simplified coupled-channel code for fusion cross sections including static nuclear deformations. *Comput. Phys. Commun.* **1989**, *54*, 409–412. [[CrossRef](#)]
26. Wong, C.Y. Interaction barrier in charged-particle nuclear reactions. *Phys. Rev. Lett.* **1973**, *31*, 766–769. [[CrossRef](#)]
27. Urazbekov, A.B.; Denikin, A.S.; Lukyanov, S.M.; Itaco, N.; Janseitov, D.; Mendibayev, K.; Burjan, V.; Kroha, V.; Mrazek, J.; Trzaska, W.; et al. Clusterization and strong coupled-channels effects in deuteron interaction with ^9Be nuclei. *J. Phys. G Nucl. Part. Phys.* **2019**, *46*, 105110. [[CrossRef](#)]
28. Hagino, K.; Takigawa, N. Subbarrier fusion reactions and many-particle quantum tunneling. *Prog. Theor. Phys.* **2012**, *128*, 1061–1106. [[CrossRef](#)]
29. Hill, D.L.; Wheeler, J.A. Nuclear constitution and the interpretation of fission phenomena. *Phys. Rev.* **1953**, *89*, 1102–1145. [[CrossRef](#)]
30. Martínez-Quiroz, E.; Aguilera, E.F.; Kolata, J.J.; Zahar, M. Sub-barrier fusion of $^{37}\text{Cl} + ^{70,72,73,74,76}\text{Ge}$. *Phys. Rev. C* **2001**, *63*, 054611. [[CrossRef](#)]
31. National Nuclear Data Center, Brookhaven National Laboratory. NuDat (Nuclear Structure and Decay Data). Available online: <https://advlabs.aapt.org/items/Load.cfm?ID=6648> (accessed on 18 March 2008).
32. Kibedi, T.; Spear, R. Reduced electric-octupole transition probabilities, $B(E3; 0_1^+ \rightarrow 3_1^-)$ —An update. *At. Data Nucl. Data Tables* **2002**, *80*, 35–82. [[CrossRef](#)]
33. Moller, P.; Sierk, A.; Ichikawa, T.; Sagawa, H. Nuclear ground-state masses and deformations: FRDM(2012). *At. Data Nucl. Data Tables* **2016**, *109*, 1–204. [[CrossRef](#)]
34. Pritychenko, B.; Birch, M.; Singh, B.; Horoi, M. Tables of E2 transition probabilities from the first 2^+ states in even-even nuclei. *At. Data Nucl. Data Tables* **2016**, *107*, 1–139. [[CrossRef](#)]
35. Raghavan, P. Table of nuclear moments. *At. Data Nucl. Data Tables* **1989**, *42*, 189–291. [[CrossRef](#)]
36. Akyuz, R.O.; Winther, A. *Course on Nuclear Structure and Heavy-Ion Reactions*; Broglia, R.A., Dasso, C.H., Ricci, R., Eds.; Enrico Fermi School of Physics: Amsterdam, The Netherlands, 1981; p. 491.